Finite-Time Adaptive Second-Order Sliding Mode Speed Control Method With Enhanced Disturbance Rejection for SPMSM

Cao Li, Tianhong Pan, *Senior Member, IEEE*, Shihong Ding, *Senior Member, IEEE*, and Liming Qian

***Abstract*—To enhance the speed tracking accuracy and robustness of surface-mounted permanent magnet synchronous motor (SPMSM) under uncertain disturbances, a new adaptive second-order sliding mode (NASOSM) speed control method is proposed. First, the dynamic model of SPMSM under uncertainties is established, a new adaptive SOSM speed controller incorporating a power integrator is constructed, which ensures the finite-time stability. Compared with the traditional fixed gain SOSM controller, the proposed controller ensures that the SPMSM maintains strong robustness against uncertainties without compromising steady-state performance, and the speed tracking error converges in finite-time to the predetermined region independent of the initial system state. By incorporating a second derivative term, the control channel uncertainty is reduced. Second, a new nonlinear disturbance observer (NDOB) is designed to estimate uncertainties in real-time. Nonlinear functions are introduced to replace the linear terms in the extended state observer accelerating the convergence of the observation error to zero, further enhancing disturbance rejection and alleviating chattering. Furthermore, the NASOSM speed controller integrated with the NDOB enhances the response speed of system state far from equilibrium, and avoids overestimation of controller gain, which is rigorously analyzed via Lyapunov theory. Finally, experimental results validate that the proposed control method significantly improves both the transient and steady-state performance of the SPMSM under various operating conditions.**

***Index Terms*—Adaptive second-order sliding mode, finite-time stability, nonlinear disturbance observer (NDOB), surface-mounted permanent magnet synchronous motor (SPMSM), uncertain disturbances.**

I. Introduction

PERMANENT magnet synchronous motors (PMSMs) have been widely adopted in industrial applications, including electric vehicles, numerical control machine tools, ship transportation, and aerospace, due to their low acoustic noise, high power density, high reliability, superior torque-current ratio, and simple structure [1], [2]. Despite these benefits, the PMSM system is inherently nonlinear, strong coupling, and susceptible to external disturbances and parameter variations [3]. Traditional proportional-integral (PI) control is commonly applied due to its easy implementation, but it is sensitive to time-varying disturbances, struggling to achieve both disturbance rejection and precise tracking [4], [5].

To address this challenge, numerous advanced nonlinear control strategies have been investigated, including fuzzy control [6], model predictive control [7], finite-time control [8], intelligent control [9], and sliding-mode control (SMC) [10], [11]. Among them, SMC is particularly effective for PMSM speed control due to its robustness and low computational complexity [12], [13], [14]. However, the classic SMC approach suffers from chattering caused by the discontinuous switching function [15], [3]. To alleviate chattering, boundary layer strategies have been explored [16], [17], which is adopted to make the control signal continuous, but the system control accuracy and disturbance rejection ability will be weakened [18]. Meanwhile, the finite-time convergence of system error cannot be guaranteed, which will limit the actual operation effect of the PMSM. Therefore, terminal sliding mode [5], [19], [20], fast integral terminal sliding mode [21], and nonsingular fast terminal sliding mode [22], [23] is proposed and applied in motor drive control, due to its strong antidisturbance capability and finite-time convergence. Although the sliding mode reaching time is reduced, it depends on the initial state of the system, which leads to the convergence time being affected when the initial state is large. Therefore, to solve this problem, some fixed-time sliding mode functions and reaching laws have been developed to ensure the independence of convergence time and initial state [24], [25]. In [25], the adaptive reaching law is introduced to reduce chattering, and a fixed-time sliding mode controller is constructed. Notably, it relies on numerous design parameters and poses certain challenges in balancing the convergence speed and robustness. Similarly, a series of predetermined time sliding mode controls are designed to guarantee the system stability at predetermined times during the arrival and sliding phases [26], [12]. In [24] and [26], the control input contains discontinuous terms. Although the reaching time is guaranteed, the task of balancing the chattering level still deserves attention. The predetermined time convergence of position tracking was achieved by introducing nonsingular terminal sliding modes and time-varying gains [12]. However,

Received 30 August 2025; revised 15 November 2025; accepted 7 January 2026. Date of publication 12 January 2026; date of current version 20 March 2026. This work was supported by the National Natural Science Foundation of China under Grant 62273002. Recommended for publication by Associate Editor J. Dong. *(Corresponding author: Tianhong Pan.)*

Cao Li and Tianhong Pan are with the School of Electrical Engineering and Automation, Anhui University, Hefei 230601, China (e-mail: z23101007@stu.ahu.edu.cn; thpan@ahu.edu.cn).

Shihong Ding is with the School of Electrical and Information Engineering, Jiangsu University, Zhenjiang 212013, China (e-mail: dsh@ujs.edu.cn).

Liming Qian is with Anhui Guoke Environment Protection Equipment Manufacturing Company Ltd., Lu'an 237000, China (e-mail: qianw@zkxtdept.com).

Color versions of one or more figures in this article are available at https://doi.org/10.1109/TPEL.2026.3653494.

Digital Object Identifier 10.1109/TPEL.2026.3653494

the disturbance is estimated by setting a positive constant, which is difficult to obtain precisely in actual systems and may lead to overestimation.

To balance chattering suppression with robustness, a second-order sliding mode (SOSM) controller has been introduced [27]. By acting on the second derivative of sliding variable and using the integral of the control signal derivative, SOSM achieves continuous control with increased relative degree, allowing both the sliding variable and its derivative to converge to zero under disturbances [28], [29]. Various SOSM-based controllers, such as super-twisting sliding mode, have been demonstrated excellent tracking and disturbance rejection capabilities in PMSMs [30], [31], [32], [33], [34]. Another SOSM constructed with the relay polynomial algorithm has a simple structure and achieves finite-time convergence [35], [36]. However, a positive constant is employed to evaluate the disturbance upper bound, which leads to the overestimate disturbance bounds and induce chattering [37]. Other approaches integrate adaptive backstepping and high-frequency switching to enhance robustness [38]. Furthermore, to suppress uncertainties, the SOSM control gain should also be reasonably designed. In recent years, to further solve the problem, several adaptive SOSM strategies have been explored [39], [40], [41], [42]. In [39], an adaptive SOSM is proposed, in which the control gain will continuously increase to reach the sliding mode. However, when encountering uncertainties, the control gain does not decrease with the variation of the disturbance, which leads to the overestimation of the disturbance. To avoid such problems, the sliding variables converge to zero neighborhood in finite time by implementing gain adaptively increasing and decreasing [40], [41]. However, the size of zero neighborhood and the convergence time depend on the upper limit of the prior uncertainty [42]. In [42], the trajectory is driven to the prespecified area by adopting the barrier function, and the area is not affected by lumped disturbances. When the sliding mode variable approaches the boundary of the area, the control input steps to infinity, which will lead to the actuator saturation problem [43]. In practical applications, there are cases where the system trajectory deviates from this region and never converges to it, which may occur in the case of switching function mutation or input saturation [44].

In actual PMSM systems, disturbances are typically unknown, it is difficult to select the upper limit value [2]. If the parameter mismatch and external disturbances can be accurately estimated, then only a small control gain needs to be set to handle the estimation error [18]. Advanced observer can estimate and compensate for these disturbances, ensuring steady-state accuracy and enhancing robustness [45]. Observer-based sliding model strategies [46], [47], such as extended state observers (ESOs), have shown effectiveness in PMSM applications. In [48], the ESO was also shown to avoid the overestimation of the switching gain when coping with disturbances. However, the estimation error of the traditional linear ESO can only be guaranteed to converge to zero asymptotically, resulting in limited observation speed and accuracy.

Motivated by the above research, this work aims to balance the response speed, disturbance rejection performance and steady-state accuracy of surface-mounted PMSM (SPMSM) speed regulation system. It is achieved by designing a new adaptive second-order sliding mode (NASOSM) controller combined with nonlinear disturbance observer (NDOB). First, the controller is designed to ensure the convergence of speed errors within a finite time, guaranteeing that speed regulation system can achieve rapid tracking in uncertain environments. Second, the designed NASOSM can avoid parameter overestimation, enabling the system to achieve excellent steady-state and dynamic performance. To further enhance the robustness of the system under uncertainty, an NDOB is designed to ensure that the estimation error can converge within a finite time, which also further accelerates the convergence speed and alleviates the problem of parameter overestimation. The main contributions are summarized as follows.

1) A NASOSM controller incorporating an adaptive strategy and power integrator is developed to suppress chattering in SPMSMs under uncertainty. This controller only requires disturbance to be bounded, excludes differential terms, and introduces uncertainty into system variable. It is more consistent than conventional SMC in the SPMSM operating environment.
2) A dynamic attraction domain is constructed using the sliding variables to adaptively tune control gains, the speed response is accelerated. The controller can achieve finite-time convergence at each case, the convergence time is independent of the initial state with a predetermined region. The adaptive gain avoids gain overestimation, further enhances the robustness of SPMSM when encountering significant disturbances.
3) An NDOB is designed to estimate system disturbances. Nonlinear terms are introduced, enhancing robustness under sudden environment changes. The designed NDOB guarantees finite-time convergence of observation errors, mitigates gain overestimation, and enhance steady state accuracy.

The rest of this article is organized as follows. Section II formulates the problem and presents preliminary lemmas. Section III details the design of NASOSM controller and NDOB. Section IV provides experimental validation. Finally, Section V concludes this article.

Notation: $sgn(p)$ is sign function, $\lfloor p \rceil^{\phi}$ is expressed as $|p|^{\phi} sgn(p)$ with $\phi > 0$, and p is any real number.

II. Problem Formulation and Preliminaries

In the d-q rotating frame, the mathematical model of SPMSM can be expressed as

$$\begin{cases} \dot{i}_d = \frac{u_d}{L} - \frac{R}{L} i_d + n_p \omega_m i_q \\ \dot{i}_q = \frac{u_q}{L} - \frac{R}{L} i_q - n_p \omega_m i_d - \frac{n_p \omega_m \psi_f}{L} \\ \dot{\omega}_m = \frac{T_e}{J} - \frac{B\omega_m}{J} - \frac{T_L}{J} \end{cases} \tag{1}$$

where i_d, u_d, and i_q, u_q are the stator current and voltages in the d-axis and q-axis, respectively, R is the stator resistance, L is the stator inductance, ω_m is the mechanical speed, ψ_f is the flux linkage, $T_e = 3n_p\psi_f i_q^*/2$ is electromagnetic torque, n_p is the number of pole pairs, J is the rotational inertia, T_L is the load torque, and B is the damping coefficient.

Considering parameter uncertainties and external disturbance, the speed control loop is rewritten as

$$\dot{\omega}_m = \frac{T_e}{J} - \frac{B\omega_m}{J} + d_0 \tag{2}$$

where $d_0 = -(T_L + \Delta B\omega_m + \Delta J\dot{\omega}_m)/J$ represents the lumped disturbance.

Under field-oriented control, traditional SMC has satisfactory performance in the speed loop control of SPMSM. However, the switching function of $sign$ affects the performance of SPMSM. To balance tracking accuracy and robustness, a NASOSM speed control scheme combined with disturbance observer is proposed for uncertain conditions.

Meanwhile, some lemmas are introduced to analyze the stability of the presented controller.

Lemma 1 [27]: If $m_1 > 0$ and $0 < m_2 < 1$, for $\forall x_1, x_2 \in R$, the following inequality holds:

$$|\lfloor x_1 \rceil^{m_1 m_2} - \lfloor x_2 \rceil^{m_1 m_2}| \le 2^{1-m_2} |\lfloor x_1 \rceil^{m_1} - \lfloor x_2 \rceil^{m_1}|^{m_2} \tag{3}$$

$$|\lfloor x_1 \rceil^{m_1} - \lfloor x_2 \rceil^{m_1}| \le 2^{\frac{1}{m_2}-1} \left| \lfloor x_1 \rceil^{\frac{m_1}{m_2}} - \lfloor x_2 \rceil^{\frac{m_1}{m_2}} \right|^{m_2}. \tag{4}$$

Lemma 2 [49]: If $k_1 > 0$, $k_2 > 0$, and n is any positive function, for $\forall x_1, x_2 \in R$, one has

$$|x_1|^{k_1} |x_2|^{k_2} \le \frac{k_1}{k_1 + k_2} n |x_1|^{k_1+k_2} + \frac{k_2}{k_1 + k_2} n^{-\frac{k_1}{k_2}} |x_2|^{k_1+k_2}. \tag{5}$$

Lemma 3 [50]: For $\forall x_i \in R, i = 1, \ldots, n$, if the real number $0 < a \le 1$, one yields

$$(|x_1| + |x_2| + \ldots + |x_n|)^a \le |x_1|^a + |x_2|^a + \ldots + |x_n|^a. \tag{6}$$

Lemma 4 [51]: If $0 < p_1 < 1$, $p_2 > 1$, x_i is positive scalar, and $i = 1, 2, \ldots, n$, then

$$\left(\sum_{i=1}^{n} |x_i| \right)^{p_1} \le \sum_{i=1}^{n} |x_i|^{p_1}, n^{1-p_2} \left(\sum_{i=1}^{n} |x_i| \right)^{p_2} \le \sum_{i=1}^{n} |x_i|^{p_2}. \tag{7}$$

Lemma 5 [52]: For a nonlinear system $\dot{x}_1 = f(x_1)$, if a Lyapunov function satisfies

$$\dot{V}(x_1) \le -l_1 V^m(x_1) - l_2 V^n(x_1) \tag{8}$$

Where $l_1 > 0, l_2 > 0, 0 < m < 1, n > 1, x \in \Re$, and $x_1(0) = x_0$. Then, the system state converges to the origin in fix-time

$$T_a \le \frac{1}{l_1(1-m)} + \frac{1}{l_2(n-1)}. \tag{9}$$

Lemma 6 [53]: For a nonlinear system $\dot{x}_2 = g(x_2)$, if a Lyapunov function satisfies

$$\dot{V}_b(x_2) \le -l_3 V_b^c(x_2) - l_4 V_b(x_2) \tag{10}$$

Where $l_3 > 0, l_4 > 0, 0 < c < 1, x_2 \in \Re$, and $g(0) = 0$. Then, system state stabilizes to the origin in a finite time

$$T_b \le \frac{1}{l_4(1-c)} \ln \frac{l_4 V_b^{1-c}[x_2(0)] + l_3}{l_3} \tag{11}$$

where $x_2(0)$ is initial state.

Lemma 7 [55]: For a nonlinear system $\dot{x}_3 = \Upsilon(x_3)$, if a Lyapunov function satisfies

$$\dot{V}_c(x_3) \le -l_5 V_c^w(x_3) - l_6 V_c^{z_1}(x_3) + l_7 \tag{12}$$

Where $l_5 > 0$, $l_6 > 0$, $0 < w < 1$, $z_1 > 1$, $0 < l_7 < \infty$, $x_3 \in \Re$, and $\Upsilon(0) = 0$. The system is practically fixed-time (T_c) stable

$$T_c \le \frac{1}{l_5 \ell(1-w)} + \frac{1}{l_6 \ell(z_1 - 1)} \tag{13}$$

where $\ell \in (0, 1)$, and the system is regulated to the residual set

$$\Xi = \left\{ \lim_{x_3 \to T_c} |V_c(x_3) \le \min \left\{ l_5^{-\frac{1}{w}} \left(\frac{l_7}{1-\ell} \right)^{\frac{1}{w}} \times l_6^{-\frac{1}{w}} \left(\frac{l_7}{1-\ell} \right)^{\frac{1}{z_1}} \right\} \right\}. \tag{14}$$

III. NASOSM Control Scheme Design

In this section, an adaptive strategy is introduced to design a SOSM controller, ensuring that the speed error converge smoothly in finite time, even in the presence of unknown lumped disturbances. In addition, to prevent gain overestimation under large disturbances, a new disturbance observer is developed to further enhance the dynamic performance of the SPMSM.

A. Design of NASOSM Controller

Define the speed tracking error

$$\varpi_e = \omega_m - \omega_m^* \tag{15}$$

where ω_m^* is the desired mechanical speed.

Taking the time derivatives of ϖ_e yields

$$\dot{\varpi}_e = \frac{K_t}{J} i_q^* - \frac{B}{J} \varpi_e + d_1 \tag{16}$$

where $d_1 = d_0 - \frac{B}{J}\omega_m^* - \dot{\omega}_m^*$, $K_t = 3n_p\psi_f/2$.

From (15) and (16), the sliding mode variables $s_1 = \varpi_e, s_2 = \frac{K_t}{J} i_q^*$ are constructed. Taking the time derivative of s_1 and s_2, $\dot{s}_1$ and $\dot{s}_2$ are rewritten as

$$\begin{cases} \dot{s}_1 = s_2 - \frac{B}{J} s_1 + d_1 \\ \dot{s}_2 = \frac{K_t}{J} u \end{cases} \tag{17}$$

where $u = \dot{i}_q^*$ is virtual control input.

Assumption 1: The d_1 is bounded, $|\dot{d}_1| \le F_d$, where F_d is unknown constant, and $F_d > 0$.

Remark 1: The same assumption is often used in the actual operation of permanent magnet synchronous motors [56], [57]. Uncertainty is usually caused by parameter mismatch and external disturbances. Both current and speed are physically constrained, then T_L, ω_m, and ω_m^* must be bounded, making Assumption 1 is reasonable.

For (17), the NASOSM controller is constructed as

$$u = -\lambda_1 \left(\left\lfloor s_2 + \hat{d}_1 \right\rceil^2 + \lambda_2^2(s_1) \cdot s_1 \right) - \hat{\mu} \cdot sign \left(\left\lfloor s_2 + \hat{d}_1 \right\rceil^2 + \lambda_2^2(s_1) \cdot s_1 \right) \tag{18}$$

$$\lambda_2(s_1) = \rho_0 + \alpha |s_1| + \frac{B}{J} |s_1|^{\frac{1}{2}} \tag{19}$$

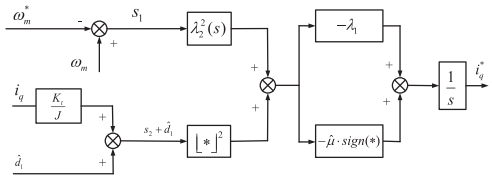

Fig. 1. NASOSM speed control for SPMSM.

$$\dot{\hat{\mu}}=\begin{cases}\frac{\rho_0}{2}|\hat{\mu}-k_2|^{\frac{1}{2}}+\alpha|\hat{\mu}-k_2|^{\frac{3}{2}}, H(s_1,\bar{s}_2)>h,\\ \quad k_1\le\hat{\mu}\le k_2\\ -\frac{\rho_0}{2}|\hat{\mu}-k_2|^{\frac{1}{2}}-\alpha|\hat{\mu}-k_2|^{\frac{3}{2}}-L_1, H(s_1,\bar{s}_2)\\ \quad \le h, k_1\le\hat{\mu}\le k_2\\ L_2, \hat{\mu}<k_1\\ 0, \hat{\mu}>k_2\end{cases} \tag{20}$$

$$H(s_1,\bar{s}_2)=\frac{2}{5}|s_1|^{\frac{5}{2}}+\frac{1}{20}\left|\bar{s}_2+\lambda_2(s_1)\cdot\lfloor s_1\rfloor^{\frac{1}{2}}\right|^5 \tag{21}$$

where $\lambda_1=\alpha J/K_t$, k_1, and k_2 are positive constants, $k_1>0$, $k_2\ge\frac{J}{K_t}[\delta(\rho_0)+\tau_3(s_1)+\frac{\rho_0}{2}+F_d]$, $\hat{d}_1$ is the estimate of d_1, $\alpha>0$, $L_1>0$, $L_2>0$,$h>0$, and $\rho_0>0$.

Remark 2: The motor parameters are changed along with the motor operates, making their variation trends difficult to predict [54]. From (16), it can be seen that both external lumped disturbances and parameter mismatches are included in d_1. The uncertainty d_1 of the proposed method is directly manifested in the controller, and accurate observation d_1 can compensate for the adverse effects caused by internal and external disturbances.

In the PMSM system, the designed NASOSM speed control block diagram is shown in Fig. 1.

Theorem 1: Under Assumption 1, the control law (18) with the adaptive update (19) and (20) guarantees finite time convergence to a predetermined region and stability of SOSM.

Proof. Step 1: Select a Lyapunov function

$$V_1(s_1)=\frac{2}{5}|s_1|^{\frac{5}{2}}. \tag{22}$$

Combined with (17), the derivative of $V_1(s_1)$ is obtained

$$\begin{aligned}\dot{V}_1(s_1)&=\lfloor s_1\rfloor^{\frac{3}{2}}\left(s_2-\frac{B}{J}s_1+\hat{d}_1\right)\\ &\le\lfloor s_1\rfloor^{\frac{3}{2}}s_2^*+\lfloor s_1\rfloor^{\frac{3}{2}}(s_2-s_2^*)+\frac{B}{J}|s_1|\,|s_1|^{\frac{3}{2}}+\lfloor s_1\rfloor^{\frac{3}{2}}d_1\end{aligned} \tag{23}$$

where s_2^* is expressed as $-\lambda_2(s_1)\cdot\lfloor s_1\rfloor^{\frac{1}{2}}-\hat{d}_1$.

Substituting s_2^* into (23), implies

$$\begin{aligned}\dot{V}_1(s_1)&\le\lfloor s_1\rfloor^{\frac{3}{2}}\left(-\rho_0-\alpha|s_1|-\frac{B}{J}|s_1|^{\frac{1}{2}}\right)\lfloor s_1\rfloor^{\frac{1}{2}}\\ &\quad+\lfloor s_1\rfloor^{\frac{3}{2}}(s_2-s_2^*)+\frac{B}{J}|s_1|^{\frac{3}{2}}|s_1|\\ &=\lfloor s_1\rfloor^{\frac{3}{2}}(s_2-s_2^*)-\rho_0 s_1^2-\alpha|s_1|^3.\end{aligned} \tag{24}$$

Step 2: Define the Lyapunov function $V_2(s_1,\bar{s}_2)$ as

$$V_2(s_1,\bar{s}_2)=V_1(s_1)+W(s_1,\bar{s}_2)+\frac{2}{5}|\hat{\mu}-k_2|^{\frac{5}{2}} \tag{25}$$

and the $W(s_1,\bar{s}_2)$ is chosen as

$$W(s_1,\bar{s}_2)=\int_{\bar{s}_2^*}^{\bar{s}_2}\left\lfloor\lfloor\xi\rfloor^2-\lfloor\bar{s}_2^*\rfloor^2\right\rfloor^2 d\xi \tag{26}$$

where $\bar{s}_2=s_2+\hat{d}_1$, $\bar{s}_2^*=s_2^*+\hat{d}_1$.

According to (24), taking derivative of $V_2(s_1,\bar{s}_2)$ yields

$$\begin{aligned}\dot{V}_2(s_1,\bar{s}_2)&=\dot{V}_1(s_1)+\frac{\partial W(s_1,\bar{s}_2)}{\partial s_1}\dot{s}_1\\ &\quad+\frac{\partial W(s_1,\bar{s}_2)}{\partial\bar{s}_2}\dot{\bar{s}}_2+\dot{\hat{\mu}}\lfloor\hat{\mu}-k_2\rfloor^{\frac{3}{2}}\\ &\le\lfloor s_1\rfloor^{\frac{3}{2}}(s_2-s_2^*)-\rho_0 s_1^2-\alpha|s_1|^3+\frac{\partial W(s_1,\bar{s}_2)}{\partial s_1}\dot{s}_1\\ &\quad+\lfloor\vartheta\rfloor^2\dot{\bar{s}}_2+\dot{\hat{\mu}}\lfloor\hat{\mu}-k_2\rfloor^{\frac{3}{2}}\end{aligned} \tag{27}$$

where $\vartheta=\lfloor\bar{s}_2\rfloor^2-\lfloor\bar{s}_2^*\rfloor^2$.

Next, each term on the right in (27) is analyzed one by one. Note that

$$|s_2-s_2^*|=|\bar{s}_2-\bar{s}_2^*|. \tag{28}$$

The Lemma 1 and 2 is applied, one has

$$\begin{aligned}\lfloor s_1\rfloor^{\frac{3}{2}}(s_2-s_2^*)&\le\sqrt{2}\left(\frac{3}{4}n_1 s_1^2+\frac{1}{4}n_1^{-3}\vartheta^2\right)\\ &\triangleq\frac{1}{4}\rho_0 s_1^2+\delta(\rho_0)\vartheta^2\end{aligned} \tag{29}$$

where $\frac{1}{4}\rho_0=\frac{3\sqrt{2}}{4}n_1$, $\delta(\rho_0)=\frac{\sqrt{2}}{4}(\frac{3\sqrt{2}}{\rho_0})^3$.

Then, $\frac{\partial W(s_1,\bar{s}_2)}{\partial s_1}\dot{s}_1$ is denoted as

$$\left|\frac{\partial W(s_1,\bar{s}_2)}{\partial s_1}\dot{s}_1\right|\le 2|\vartheta|\,|\bar{s}_2-\bar{s}_2^*|\left|\frac{\partial\lfloor\bar{s}_2^*\rfloor^2}{\partial s_1}\dot{s}_1\right|. \tag{30}$$

By Lemma 1, it can be deduced as

$$\left|\frac{\partial\lfloor\bar{s}_2^*\rfloor^2}{\partial s_1}\right|=\left|\frac{\partial\left[\lambda_2^2(s_1)\right]}{\partial s_1}s_1\right|+\lambda_2^2(s_1). \tag{31}$$

And based on $\bar{s}_2=s_2+\hat{d}_1$ and Lemma 1, $\bar{s}_2$ can be obtained that

$$\begin{aligned}\bar{s}_2&=(s_2-s_2^*)+s_2^*+\hat{d}_1\\ &\le|\bar{s}_2-\bar{s}_2^*|+\left|s_2^*+\hat{d}_1\right|\\ &\le\sqrt{2}|\vartheta|^{\frac{1}{2}}+\lambda_2(s_1)\cdot|s_1|^{\frac{1}{2}}.\end{aligned} \tag{32}$$

Together with $\dot{s}_1$ and (32), implies

$$\begin{aligned}|\dot{s}_1|&=\left|\bar{s}_2-\frac{B}{J}s_1\right|\\ &\le\left|\sqrt{2}|\vartheta|^{\frac{1}{2}}+\lambda_2(s_1)\cdot|s_1|^{\frac{1}{2}}-\frac{B}{J}s_1\right|\\ &=\sqrt{2}|\vartheta|^{\frac{1}{2}}+\left[\lambda_2(s_1)+\frac{B}{J}|s_1|^{\frac{1}{2}}\right]|s_1|^{\frac{1}{2}}.\end{aligned} \tag{33}$$

Furthermore, $|\frac{\partial\lfloor\bar{s}_2^*\rfloor^2}{\partial s_1}\dot{s}_1|$ can be transformed into

$$\left|\frac{\partial\lfloor\bar{s}_2^*\rfloor^2}{\partial s_1}\dot{s}_1\right|\le\left|\left(\left|\frac{\partial\left[\lambda_2^2(s_1)\right]}{\partial s_1}s_1\right|+\lambda_2^2(s_1)\right)\right.$$

$$\times\left[\sqrt{2}|\vartheta|^{\frac{1}{2}}+\left(\lambda_2(s_1)+\frac{B}{J}|s_1|^{\frac{1}{2}}\right)|s_1|^{\frac{1}{2}}\right]\Bigg|$$
$$=\left[\sqrt{2}\left|\frac{\partial\left[\lambda_2^2(s_1)\right]}{\partial s_1}s_1\right|+\sqrt{2}\lambda_2^2(s_1)\right]|\vartheta|^{\frac{1}{2}}$$
$$+\left(\lambda_2(s_1)+\frac{B}{J}|s_1|^{\frac{1}{2}}\right)\left[\left|\frac{\partial\left[\lambda_2^2(s_1)\right]}{\partial s_1}s_1\right|+\lambda_2^2(s_1)\right]|s_1|^{\frac{1}{2}}. \tag{34}$$

It can be determined that

$$\left|\frac{\partial\lfloor\bar{s}_2^*\rfloor^2}{\partial s_1}\dot{s}_1\right|\le\tau_1(s_1)|s_1|^{\frac{1}{2}}+\tau_2(s_1)|\vartheta|^{\frac{1}{2}} \tag{35}$$

$$\tau_1(s_1)=\left(\lambda_2(s_1)+\frac{B}{J}|s_1|^{\frac{1}{2}}\right)\left[\left|\frac{\partial\left[\lambda_2^2(s_1)\right]}{\partial s_1}s_1\right|+\lambda_2^2(s_1)\right] \tag{36}$$

$$\tau_2(s_1)=\sqrt{2}\left|\frac{\partial\left[\lambda_2^2(s_1)\right]}{\partial s_1}s_1\right|+\sqrt{2}\lambda_2^2(s_1). \tag{37}$$

Combining (30), (35) and Lemma 1 obtains

$$\left|\frac{\partial W(s_1,\bar{s}_2)}{\partial s_1}\dot{s}_1\right|\le 2^{\frac{3}{2}}|\vartheta|^{\frac{3}{2}}\left(\tau_1(s_1)|s_1|^{\frac{1}{2}}+\tau_2(s_1)|\vartheta|^{\frac{1}{2}}\right). \tag{38}$$

Applying Lemma 2, then (38) can be rewritten as

$$\begin{aligned}\left|\frac{\partial W(s_1,\bar{s}_2)}{\partial s_1}\dot{s}_1\right|&\le 2^{\frac{3}{2}}\tau_1(s_1)\frac{1}{4}n_2s_1^2\\&\quad+2^{\frac{3}{2}}\left[\tau_1(s_1)\frac{3}{4}n_2^{-\frac{1}{3}}+\tau_2(s_1)\right]\vartheta^2\\&\triangleq\frac{1}{4}\rho_0s_1^2+\tau_3(s_1)\vartheta^2\end{aligned} \tag{39}$$

where $\rho_0=2^{\frac{3}{2}}\tau_1(s_1)n_2$, $\tau_3(s_1)=[3\tau_1^{\frac{4}{3}}(s_1)+2^{\frac{3}{2}}\tau_2(s_1)]\rho_0^{-\frac{1}{3}}$.

The $\dot{V}_2(s_1,s_2)$ can be transformed into

$$\begin{aligned}\dot{V}_2(s_1,\bar{s}_2)\le&-\frac{1}{2}\rho_0s_1^2-\alpha|s_1|^3+\lfloor\vartheta\rfloor^2\left[\frac{K_t}{J}u+\dot{\hat{d}}_1\right]\\&+\left[\delta(\rho_0)+\tau_3(s_1)\right]\vartheta^2+\dot{\hat{\mu}}\lfloor\hat{\mu}-k_2\rfloor^{\frac{3}{2}}.\end{aligned} \tag{40}$$

Hence, the controller u is constructed as

$$u=-\lambda_1\vartheta-\hat{\mu}\cdot sign(\vartheta) \tag{41}$$

where $\hat{\mu}\ge\frac{J}{K_t}[\delta(\rho_0)+\tau_3(s_1)+F_d+\frac{\rho_0}{2}]$.

Combining (40) and (41) can be calculated as

$$\begin{aligned}\dot{V}_2(s_1,\bar{s}_2)\le&-\frac{\rho_0}{2}\left[s_1^2+\vartheta^2+(\hat{\mu}-k_2)^2\right]\\&+\dot{\hat{\mu}}\lfloor\hat{\mu}-k_2\rfloor^{\frac{3}{2}}-\alpha|s_1|^3\\&-\alpha|\vartheta|^3-\alpha|\hat{\mu}-k_2|^3+\frac{\rho_0}{2}(\hat{\mu}-k_2)^2+\alpha|\hat{\mu}-k_2|^3.\end{aligned} \tag{42}$$

Therefore, $V_2(s_1,s_2)$ can be estimated as

$$V_2(s_1,\bar{s}_2)\le 2\left(|s_1|^{\frac{5}{2}}+|\vartheta|^{\frac{5}{2}}+|\hat{\mu}-k_2|^{\frac{5}{2}}\right). \tag{43}$$

Applying Lemma 3 to (43) yields

$$V_2^{\frac{4}{5}}(s_1,\bar{s}_2)\le 2^{\frac{4}{5}}\left(|s_1|^2+|\vartheta|^2+|\hat{\mu}-k_2|^2\right). \tag{44}$$

By applying Lemma 4 to (43), it can also be obtained that

$$\begin{aligned}V_2^{\frac{6}{5}}(s_1,\bar{s}_2)&\le 2^{\frac{6}{5}}\left(|s_1|^{\frac{5}{2}}+|\vartheta|^{\frac{5}{2}}+|\hat{\mu}-k_2|^{\frac{5}{2}}\right)^{\frac{2}{5}\times3}\\&=2^{\frac{16}{5}}\left(|s_1|^3+|\vartheta|^3+|\hat{\mu}-k_2|^3\right).\end{aligned} \tag{45}$$

Let $\chi_1=\rho_0/2^{\frac{9}{5}}$, $\chi_2=\alpha/2^{\frac{16}{5}}$, one yields

$$\dot{V}_2(s_1,\bar{s}_2)+\chi_1V_2^{\frac{4}{5}}(s_1,\bar{s}_2)+\chi_2V_2^{\frac{6}{5}}(s_1,\bar{s}_2)\le q \tag{46}$$

where $q=\dot{\hat{\mu}}\lfloor\hat{\mu}-k_2\rfloor^{\frac{3}{2}}+\frac{\rho_0}{2}(\hat{\mu}-k_2)^2+\alpha|\hat{\mu}-k_2|^3$.

Case I: Provide $H(s_1,\bar{s}_2)>h$ and $k_1\le\hat{\mu}\le k_2$, then, the adaptive law is reduced to

$$\dot{\hat{\mu}}=\frac{\rho_0}{2}|\hat{\mu}-k_2|^{\frac{1}{2}}+\alpha|\hat{\mu}-k_2|^{\frac{3}{2}} \tag{47}$$

which leads to $q=0$ in (46).

When $\frac{J}{K_t}[\delta(\rho_0)+\tau_3(s_1)+\frac{\rho_0}{2}+F_d]\le\hat{\mu}\le k_2$, one has

$$\dot{V}_2(s_1,\bar{s}_2)\le-\chi_1V_2^{\frac{4}{5}}(s_1,\bar{s}_2)-\chi_2V_2^{\frac{6}{5}}(s_1,\bar{s}_2) \tag{48}$$

where $\chi_1>0$, $\chi_2>0$.

From Lemma 5, the proposed controller can be stable in a finite time to the domain $\Omega_1=\{(s_1,\bar{s}_2):H(s_1,\bar{s}_2)\le h\}$, and the time t_1 is set as

$$t_1\le\frac{5}{\chi_1}+\frac{5}{\chi_2}. \tag{49}$$

When $k_1\le\hat{\mu}<\frac{J}{K_t}[\delta(\rho_0)+\tau_3(s_1)+\frac{\rho_0}{2}+F_d]$, the $\hat{\mu}$ will increase until $\hat{\mu}\ge\frac{J}{K_t}[\delta(\rho_0)+\tau_3(s_1)+\frac{\rho_0}{2}+F_d]$ holds, the finite-time convergence has also been proved.

Remark 3: Throughout this process, $\hat{\mu}$ is always satisfies $k_1\le\hat{\mu}\le k_2$. Since k_1 and k_2 are preset constants. After adjustment with the adaptive term (47), the maximum possible time t_2 that meets the above conditions is also the time when k_1 reaches k_2. Equation (47) is associated only with $\hat{\mu}$, ρ_0 and k_2, t_2 is also independent of the system state. Increasing these values can accelerate the convergence rate, but overshoot may occur. In this case, the maximum convergence time will not exceed t_1+t_2.

Case II: Provide $H(s_1,\bar{s}_2)\le h$ and $k_1\le\hat{\mu}\le k_2$, then, the adaptive law is reduced to

$$\dot{\hat{\mu}}=-\frac{\rho_0}{2}|\hat{\mu}-k_2|^{\frac{1}{2}}-\alpha|\hat{\mu}-k_2|^{\frac{3}{2}}-L_1 \tag{50}$$

which implies that $q=-L_1\lfloor\hat{\mu}-k_2\rfloor^{\frac{3}{2}}\ge0$.When $q=0$, the sliding variables will still stay in the domain Ω_1. While $q>0$, $\hat{\mu}$ will decrease. From (40), the derivative of $V_3(s_1,\bar{s}_2)=V_1(s_1)+W(s_1,\bar{s}_2)$ is calculated

$$\begin{aligned}\dot{V}_3(s_1,\bar{s}_2)\le&-\frac{1}{2}\rho_0s_1^2-\alpha|s_1|^3+\lfloor\vartheta\rfloor^2\left[\frac{K_tu}{J}+\dot{\hat{d}}_1\right]\\&+\left[\delta(\rho_0)+\tau_3(s_1)\right]\vartheta^2\\\le&-\frac{1}{2}\rho_0s_1^2-\alpha|s_1|^3-\alpha|\vartheta|^3\\&+\vartheta^2\left[-\frac{K_t}{J}\hat{\mu}+\delta(\rho_0)+\tau_3(s_1)+F_d\right].\end{aligned} \tag{51}$$

It can be seen that the size of $\hat{\mu}$ will affect the sign of $\dot{V}_3(s_1,\bar{s}_2)$. Since both $V_3(s_1,\bar{s}_2)$ and $H(s_1,\bar{s}_2)$ contain homogeneity of degree 5/2 with respect to the dilation $(1,1/2)$, if $\hat{\mu}$ is small, increasing $V_3(s_1,\bar{s}_2)$ may cause the $H(s_1,\bar{s}_2)$ to be

greater than h, and $\dot{\hat{\mu}}$ is steered into *Case I* to achieve fixed-time convergence before $\hat{\mu}$ has decreased to k_1. If it does not cause $H(s_1, \bar{s}_2)$ greater than h, it continues to decrease until it switches to *Case III*. According to (50), even if directly reaching *Case III*, the maximum time t_3 for this phase is the duration for k_2 to approach $k_1 - a$, a is a small constant.

Remark 4: Under the premise that $k_1 > 0$, the increase of ρ_0, α, and L_1 can accelerate the convergence process of this stage, but if it is too large, it may cause unstable fluctuations in the steady state.

Case III: Assuming that $\hat{\mu} < k_1$, $\dot{\hat{\mu}}$ is represented as L_2. Then, $\hat{\mu}$ will be increased rapidly until $H(s_1, \bar{s}_2) \le h$ always holds, the proof is complete. Otherwise, the system trajectory is adjusted through *Case I* or *II*.

Remark 5: Here, L_2 determines the process that $\hat{\mu}$ reaches k_1. It should be set appropriately to ensure rapid arrival at k_1 without escaping it.

Case IV: Assuming that $\hat{\mu} > k_2$, $\dot{\hat{\mu}}$ is represented as 0. Then, the assumption is never true, $\hat{\mu}$ may reach k_2, but never exceed k_2. In this case $\hat{\mu} = k_2$ holds, depending on whether the system status is within Ω_1. If it is not satisfied $\Omega_1 = \{(s_1, \bar{s}_2) : H(s_1, \bar{s}_2) \le h\}$, the states will be converged to Ω_1 in finite time, and it will be adjusted through *Case II*. Otherwise, it directly enters *Case II*.

Remark 6: In *Case I*, $\hat{\mu}$ may result in $\hat{\mu} > k_2$. Once $\hat{\mu} > k_2$ occurs, $\dot{\hat{\mu}}$ is immediately set to 0, $\hat{\mu} = k_2$ is output to ensure that the system strictly operates within the specified range.

By (46), the q is related to ρ_0, α, $\hat{\mu}$, and k_2, these are all bounded, there must exists a positive constant $l > 0$ such that

$$\dot{V}_2(s_1, \bar{s}_2) \le -\chi_1 V_2^{\frac{4}{5}}(s_1, \bar{s}_2) - \chi_2 V_2^{\frac{6}{5}}(s_1, \bar{s}_2) + l \tag{52}$$

where $\chi_1 > 0$, $\chi_2 > 0$.

According to Lemma 7, it means $V_2(s_1, \bar{s}_2)$ will be regulated

$$V_2(s_1, \bar{s}_2) \le \min\left\{\chi_1^{-\frac{5}{4}}\left(\frac{l}{1-\ell}\right)^{\frac{5}{4}}, \chi_2^{-\frac{5}{4}}\left(\frac{l}{1-\ell}\right)^{\frac{5}{6}}\right\} \tag{53}$$

where $0 < \ell < 1$. Combining (25), (26), and Lemma 1, the $W(s_1, \bar{s}_2)$ can be obtained

$$W(s_1, \bar{s}_2) = \int_{\bar{s}_2^*}^{\bar{s}_2} \left\lfloor \lfloor \xi \rceil^2 - \lfloor \bar{s}_2^* \rceil^2 \right\rfloor^2 d\xi \ge \frac{1}{20}|\bar{s}_2 - \bar{s}_2^*|^5. \tag{54}$$

Then, one can get

$$\begin{aligned} V_1(s_1) + W(s_1, \bar{s}_2) &\ge \frac{2}{5}|s_1|^{\frac{5}{2}} + \frac{1}{20}|\bar{s}_2 - \bar{s}_2^*|^5 \\ &= H(s_1, \bar{s}_2). \end{aligned} \tag{55}$$

Furthermore, $V_2(s_1, \bar{s}_2) \ge H(s_1, \bar{s}_2)$ is true, and it will be satisfied after time t_2

$$H(s_1, \bar{s}_2) \le \min\left\{\chi_1^{-\frac{5}{4}}\left(\frac{l}{1-\ell}\right)^{\frac{5}{4}}, \chi_2^{-\frac{5}{4}}\left(\frac{l}{1-\ell}\right)^{\frac{5}{6}}\right\}. \tag{56}$$

From (25), (53), and (56), the convergence region of the system state is calculated as

$$\begin{aligned} \Omega_2 = \Bigg\{ \underset{t\to t_4}{(s_1, \bar{s}_2)} : |s_1| \le \Bigg(& \frac{5}{2}\min\left\{\chi_1^{-\frac{5}{4}}\left(\frac{l}{1-\ell}\right)^{\frac{5}{4}}, \right. \\ & \left. \chi_2^{-\frac{5}{4}}\left(\frac{l}{1-\ell}\right)^{\frac{5}{6}}\right\}\Bigg)^{\frac{2}{5}} = \upsilon_1, \\ |\bar{s}_2| \le & \left(\min\left\{\chi_1^{-\frac{5}{4}}\left(\frac{l}{1-\ell}\right)^{\frac{5}{4}}, \chi_2^{-\frac{5}{4}}\left(\frac{l}{1-\ell}\right)^{\frac{5}{6}}\right\}\right. \\ & \left. \times \left(\frac{1}{4} + \frac{5}{2}\lambda_2^5(s_1)\right)\right)^{\frac{1}{5}} = \upsilon_2 \Bigg\}. \end{aligned} \tag{57}$$

This time t_4 can be expressed as

$$t_4 \le \frac{5}{\chi_1 \ell} + \frac{5}{\chi_2 \ell} \tag{58}$$

where t_4 is setting time.

Remark 7: Through the abovementioned analysis, it can be inferred that $(s_1, \bar{s}_2)$ initially converges to the field Ω_1 in finite time, and this time is independent of the initial state. Even if it may expand to Ω_1, it remains independent of the initial state during the convergence to a broader field Ω_2. This is followed by a convergence phase, and it returns to Ω_1. In general, sliding variables are always included in the field Ω_2.

Remark 8: For *Case I*, according to (21), (49), and (58), it can be known that the increase of ρ_0 and α can reduce the maximum time in this stage. For *Case II* or *III*, from (18), (20), and (46), increasing ρ_0, α, and k_2 directly increases the values of μ and λ_1, thereby accelerating the system response speed and robustness. However, excessively large μ and λ_1 may exacerbate chattering. When *Case III* changes to *Case I* or *II*, the size of k_1 will affect the steady-state and antidisturbance performance of the controller, an excessively small k_1 may slow down the system response when the operating conditions change. It is worth noting that the initial value of $\hat{\mu}_0$ must satisfy $\hat{\mu}_0 \ge k_1$. This ensures that the motor only operates at *Case I* or *II* when it starts to run. For the adaptive term in (19), it is also necessary to observe that the ρ_0 and α will be associated with the k_2, which needs to balance the chattering and robustness under the premise of ensuring the system stability. From (57), it can be seen that ρ_0 and α will enhance the influence of system variables and expand the range of Ω_2, excessive ρ_0 and α may cause speed fluctuations. When parameter mismatch occurs, it can be known from (21) and (57) that Ω_2 and $H(s_1, \bar{s}_2)$ will be affected. Especially when the moment of inertia J is mismatched, the actual output of the controller is changed due to the variations in λ_1 and $\bar{s}_2$. However, from the convergence region Ω_2, it can be seen that only the range of $\bar{s}_2$ is affected. Since $\bar{s}_2$ is defined as $s_2 + \hat{d}_1$, if $\hat{d}_1$ is accurately obtained, the influence of parameter mismatch will be reduced.

Remark 9: The finite-time convergence of the proposed control scheme is rooted in the theory of homogeneity. For permanent magnet synchronous motor systems, due to the limitations of physical conditions, the motor speed has a limit, and $|s_1|$ must be bounded. The symbol of s_1 is not affected by $\lambda_2(s_1)$, $\lambda_2(s_1)$ can be understood as a relatively large positive constant. Thus, the control law (18) renders homogeneous of degree $-1/2$ with respect to the dilation $(1, 1/2)$, the weight of s_1 is 1, and the weight of $\bar{s}_2$ is $1/2$. According to (55), $H(s_1, \bar{s}_2)$ contain homogeneity of degree $5/2$ with respect to the dilation $(1, 1/2)$.

This deliberate construction ensures that the time derivative of the Lyapunov function along the system trajectories satisfies $\dot{V}_2(s_1,\bar{s}_2)+\chi_1 V_2^{\frac{4}{5}}(s_1,\bar{s}_2)+\chi_2 V_2^{\frac{6}{5}}(s_1,\bar{s}_2)\le q$. Through (52)–(58), the homogeneity of the closed-loop system and the Lyapunov functions not incidental.

Remark 10: The abovementioned analysis verified that NASOSM can converge to a predetermined region Ω_2 within t_4, and then further converge to region Ω_1 through various cases. The proposed control method employs an adaptive gain ($\hat{\mu}$) mechanism that dynamically adjust in response to changes in the system state, thereby avoiding the issue of parameter overestimation. Compared to conventional SOSM, NASOSM dynamically adjusts control gain in real time as the attraction domain changes. Different from the existing adaptive SOSM [42], [41], [58], the convergence time of NASOSM is independent of the initial state, thereby improving the convergence speed for large initial errors.

Remark 11: This controller enhances the system's dynamic and steady-state performance, but it does not cause the system state to converge completely to zero. The system state switches various situations under the guidance of the attraction domain to converge to a certain region, and this process has temporary discontinuities. By introducing a variable gain strategy and designing an observer, the method can effectively reduce chattering and further improves both the response speed and control accuracy.

B. Design of Nonlinear Disturbance Observer

In (16), the lumped disturbance degrades the operational performance of SPMSM. To compensate for these unknown disturbances and improve the system's robustness, a NDOB is designed in this section.

Based on the ESO in [47], nonlinear terms are introduced. The following NDOB is designed as:

$$\begin{cases}\dot{\hat{\varpi}}_e=\frac{K_t}{J}i_q-\frac{B\hat{\varpi}_e}{J}+\hat{d}_1-\varepsilon_1 f_1(\varphi_1)\\ \dot{\hat{d}}_1=-\varepsilon_2 f_2(\varphi_1)\end{cases}\tag{59}$$

$$\begin{cases}f_1(\varphi_1)=\left\lfloor\frac{\varphi_1}{\phi_2}\right\rfloor^{\phi_1}+\left\lfloor\frac{\varphi_1}{\phi_2}\right\rfloor\\ f_2(\varphi_1)=\frac{\phi_1}{\phi_2}\left\lfloor\frac{\varphi_1}{\phi_2}\right\rfloor^{2\phi_1-1}+\frac{1}{\phi_2}\left\lfloor\frac{\varphi_1}{\phi_2}\right\rfloor+\left(\frac{\phi_1+1}{\phi_2}\right)\left\lfloor\frac{\varphi_1}{\phi_2}\right\rfloor^{\phi_1}\end{cases}\tag{60}$$

where $\varphi_1=\hat{\varpi}_e-\varpi_e$, $\varepsilon_1>0$, $\varepsilon_2>0$, $\frac{1}{3}<\phi_1<1$, and $\phi_2>0$.

Accordingly, the block diagram of the designed NDOB is shown in Fig. 2.

Combining (16) and (59) yields

$$\begin{cases}\dot{\varphi}_1=\varphi_2-\varepsilon_1 f_1(\varphi_1)-\frac{B}{J}\varphi_1\\ \dot{\varphi}_2=-\varepsilon_2 f_2(\varphi_1)-\dot{d}_1\end{cases}\tag{61}$$

where $\varphi_2=\hat{d}_1-d_1$.

Then, the $\Delta(\gamma,\sigma)$ is established [59], and the inequality is satisfied

$$\Delta(\gamma,\sigma)=\begin{bmatrix}\gamma\\ \sigma\end{bmatrix}^T\begin{bmatrix}Q & K^T\\ K & -\theta I\end{bmatrix}\begin{bmatrix}\gamma\\ \sigma\end{bmatrix}\ge 0\tag{62}$$

where $\theta\ge 0$, Q, and K are two matrices, and $Q>0$.

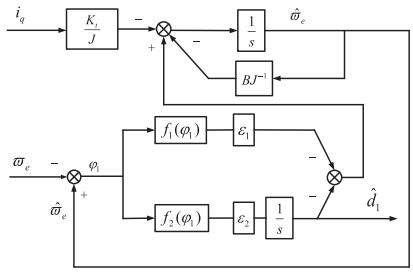

Fig. 2. NDOB for SPMSM.

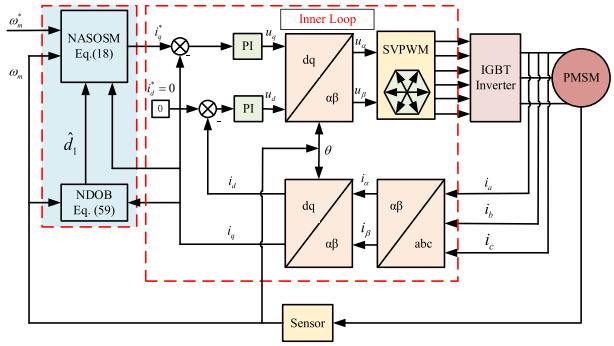

Fig. 3. Proposed NASOSM + NDOB for SPMSM.

Theorem 2: Suppose there exists the following matrix inequality:

$$\begin{bmatrix}A^TP+PA+\kappa P+Q & PD+K^T\\ D^TP+K & -\theta I\end{bmatrix}\le 0.\tag{63}$$

Then, the observation errors φ_1 will converge to 0 in a finite time. Where P is a symmetric and positive definite matrix $\kappa>0$.

Remark 12: From (62) and (63), it can be known that if A is a Hurwitz matrix and P is a symmetric and positive definite matrix, for $Q>0$, there always exists a positive constant κ such that the (63) holds. Since the matrix A of the observer error system is Hurwitz stable, this (63) always has a solution.

Proof: Define a Lyapunov function as

$$V_4(\varphi_1)=\gamma^T P\gamma\tag{64}$$

Where $\gamma^T=\begin{bmatrix}f_1(\varphi_1) & \varphi_2-\frac{B}{J}\varphi_1\end{bmatrix}$, and $P=\begin{bmatrix}\varepsilon_1^2+4\varepsilon_2 & -\varepsilon_1\\ -\varepsilon_1 & 2\end{bmatrix}$.

According to (60) and (61), $\dot{\gamma}$ is denoted as

$$\begin{aligned}\dot{\gamma}&=\begin{bmatrix}f_1'(\varphi_1)\dot{\varphi}_1\\ -\varepsilon_2 f_2(\varphi_1)-\frac{B}{J}-\dot{d}_1\end{bmatrix}\\ &=F(\varphi_1)\left(A\gamma+D\sigma\right)\end{aligned}\tag{65}$$

where $F(\varphi_1)=\frac{\phi_1}{\phi_2}\left|\frac{\varphi_1}{\phi_2}\right|^{\phi_1-1}+\frac{1}{\phi_2}$, $\sigma=-(\frac{B}{J}+\dot{\hat{d}}_1)/F(\varphi_1)$, $A=\begin{bmatrix}-\varepsilon_1 & 1\\ -\varepsilon_2 & 0\end{bmatrix}$, and $D=\begin{bmatrix}0\\ 1\end{bmatrix}$.

The derivative of $\dot{V}_3(\varphi_1)$ is

$$\begin{aligned}\dot{V}_4(\varphi_1)&=\dot{\gamma}^T P\gamma+\gamma^T P\dot{\gamma}\\ &=F(\varphi_1)\left[\gamma^T A^T P\gamma+\sigma^T D^T P\gamma+\gamma^T PA\gamma+\gamma^T PD\sigma\right]\\ &=F(\varphi_1)\left[\gamma^T\left(A^TP+PA\right)\gamma+\sigma D^TP\gamma+\sigma\gamma^TPD\right]\end{aligned}$$

$$= F(\varphi_1)\left\{\begin{bmatrix}\gamma\\ \sigma\end{bmatrix}^T\begin{bmatrix}A^TP+PA & PD\\ D^TP & 0\end{bmatrix}\begin{bmatrix}\gamma\\ \sigma\end{bmatrix}\right\}$$

$$\le F(\varphi_1)\left\{\begin{bmatrix}\gamma\\ \sigma\end{bmatrix}^T\begin{bmatrix}A^TP+PA & PD\\ D^TP & 0\end{bmatrix}\begin{bmatrix}\gamma\\ \sigma\end{bmatrix}+\Delta(\gamma,\sigma)\right\}$$

$$\le F(\varphi_1)\begin{bmatrix}\gamma\\ \sigma\end{bmatrix}^T\begin{bmatrix}-\kappa P & 0\\ 0 & 0\end{bmatrix}\begin{bmatrix}\gamma\\ \sigma\end{bmatrix}$$

$$= -\kappa\frac{\phi_1}{\phi_2}\left|\frac{\varphi_1}{\phi_2}\right|^{\phi_1-1}V_4-\kappa\frac{1}{\phi_2}V_4. \tag{66}$$

According to (64), one obtains

$$\lambda_{\min}(P)\|\gamma\|^2\le\gamma^TP\gamma\le\lambda_{\max}(P)\|\gamma\|^2. \tag{67}$$

By simple calculations, one gets

$$\|\gamma\|^2 = {f_1}^2(\varphi_1)+\left(\varphi_2-\frac{B}{J}\varphi_1\right)^2$$

$$= \left|\frac{\varphi_1}{\phi_2}\right|^{2\phi_1}+\left|\frac{\varphi_1}{\phi_2}\right|^2+2\left|\frac{\varphi_1}{\phi_2}\right|^{\phi_1+1}+{\varphi_2}^2+\left(\frac{B}{J}\varphi_1\right)^2$$

$$-2\frac{B}{J}\varphi_1\varphi_2. \tag{68}$$

From (67) and (68), we can derive

$$\left|\frac{\varphi_1}{\phi_2}\right|^{1-\phi_1}=\left(\left|\frac{\varphi_1}{\phi_2}\right|^{\phi_1}\right)^{\frac{1-\phi_1}{\phi_1}}\le\|\gamma\|^{\frac{1-\phi_1}{\phi_1}}\le\frac{1}{\lambda_{\min}^{\frac{1-\phi_1}{2\phi_1}}(P)}{V_4}^{\frac{1-\phi_1}{2\phi_1}}. \tag{69}$$

Thus, $\dot{V}_3$ can be collated as

$$\dot{V}_4\le-\phi_1\kappa\left|\frac{\varphi_1}{\phi_2}\right|^{\phi_1-1}V_4-\kappa\frac{1}{|\phi_2|}V_4$$

$$\le-\phi_1\kappa\lambda_{\min}^{\frac{1-\phi_1}{2\phi_1}}(P)V_4^{\frac{3\phi_1-1}{2\phi_1}}-\kappa\frac{1}{|\phi_2|}V_4. \tag{70}$$

According to Lemma 6, if $\phi_1\in(\frac{1}{3},1)$ is always satisfied, the designed observer is finite-time stability, and the convergence time can be expressed as

$$t_2\le\frac{\phi_2}{\kappa(1-\frac{3\phi_1-1}{2\phi_1})}\ln\frac{\frac{\kappa}{\phi_2}V_4^{1-\frac{3\phi_1-1}{2\phi_1}}[V_4(0)]+\phi_1\kappa\lambda_{\min}^{\frac{1-\phi_1}{2\phi_1}}(P)}{\phi_1\kappa\lambda_{\min}^{\frac{1-\phi_1}{2\phi_1}}(P)}. \tag{71}$$

Remark 13: The proposed observer is different from the traditional linear observer [48]. It can achieve the convergence of the observation error to 0 within a finite time, improving the observation speed and accuracy. Different from the extended sliding mode observer in [60], NDOB eliminates discontinuous terms, which reduces unnecessary chattering. The introduced nonlinear term enhances the suppression ability when dealing with motor parameter mismatch and external disturbances. By adjusting the observation bandwidth and ϕ_2, the observation speed and noise of the NDOB can be balanced, making it more suitable for practical engineering applications.

Therefore, the block diagram of NASOSM speed controller with composite NDOB can be designed, as shown in Fig. 3.

Remark 14: Chattering is originated from the high-frequency switching inherent in discontinuous control laws. In SOSM control, while the direct integration of the discontinuous term $sign(.)$ yields a continuous control signal, the underlying switching dynamics persist in the system's higher-order derivatives. The amplitude of this chattering is directly proportional to the gain coefficient of the $sign(.)$. Traditional SOSM [35], a fixed and sufficiently large gain is set to dominate unknown uncertainties, leading to gain overestimation and exacerbated steady-state chattering. The proposed adaptive strategy circumvents this issue, which is dynamically tuned via a Lyapunov-based adaptive law. The mechanism ensures a high gain for rapid convergence during transients while automatically lowering the gain near steady state, thus attenuating chattering from its root cause without sacrificing robustness. Furthermore, a comparative analysis of the observers reveals that the ESO guarantees merely asymptotic error convergence, NDOB achieves finite-time convergence to zero through rigorous Lyapunov stability analysis. This attribute of the NDOB more effectively mitigates performance degradation caused by observation errors, leading to smoother overall control.

C. Parameter Selection Guidance

To achieve the optimal performance of SPMSM in actual operation, it is necessary to set the controller's parameters reasonably. The simplified steps are described as follows.

1) *The Initial Operation of the Motor:* According to (41) and relevant constraints, $\hat{\mu}$ is first regarded as a constant μ_1, and μ, α and ρ_0 are selected to ensure that the motor satisfies the tracking requirements.
2) *Set the Adaptive Items:* Let $k_1=\mu_1$, k_2 is chosen as the maximum threshold, ρ_0, α, L_1, and L_2 are set to prompt the error to reach the predetermined area at a certain rate.
3) *Fine-Tuning for Performance:* k_1 affect the steady-state performance, and too small value may affect the disturbance rejection. k_2, α, and ρ_0 can promote the convergence speed and robustness, too large k_2 may produce overshoot. The increase of α and ρ_0 will also cause chattering.
4) *Final Adjustment:* The parameters are fine-tuned by comprehensively considering the steady-state accuracy, anti-interference and convergence time of the motor operation to achieve the optimal performance.

IV. Experiments

To validate the performance of the NASOSM + NDOB, experiments were conducted on a SPMSM, including a test motor and a load motor. The specific internal parameters of the test motor are shown in Table I. As illustrated in Fig. 4, the experimental platform includes the SPMSM, host computer, control board (TMS320F28379D), driver (DRV8305), torque sensor and power source. The sampling frequencies of the speed and current loop are 1 kHz and 10 kHz, respectively.

To assess performance, the proposed NASOSM + NDOB was compared against four benchmark controllers: PI controller, PI + NDOB, ISM controller [10], SOSM controller [35], continuous adaptive fast terminal sliding mode (CAFTSM) + NDOB [13], and NASOSM + ESO. These control schemes were applied in the speed control of SPMSM. Meanwhile, in order to verify

TABLE I
PARAMETERS OF SPMSM

Symbol	Name	Value
N_r	Rated speed	3000 r/min
T_r	Rated torque	1.27 N·m
P_r	Rated power	400 W
ψ_f	Flux linkage	0.026 Wb
J	Rotational inertia	3.86×10^{-5} kg/m^2
L	Stator inductance	0.52 mH
R	Stator resistance	0.32 Ω
B	friction coefficient	3.65×10^{-5} N·m·s
n_p	Number of poles	5

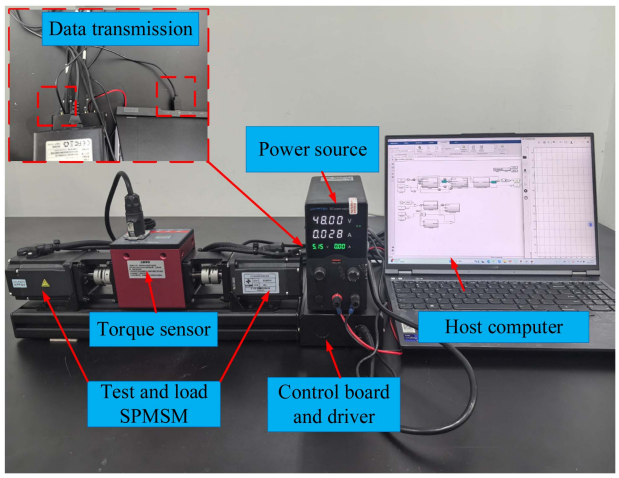

Fig. 4. Experimental platform.

the performance of the adaptive term and the observer, the comparative experiments of SOSM + ESO, SOSM + NDOB, NASOSM + ESO, and NASOSM + NDOB were carried out. The speed and q-axis current were recorded in various dynamic and steady-state conditions, including start-up, sudden load disturbances, acceleration and deceleration, rated speed and noise, and uncertainty under parameter mismatch.

The ISM controller is selected as [10]

$$i_q^* = -\frac{J}{K_t}\left[\left(c_1 - \frac{B}{J}\right)s_1\right] - m \cdot sign(s_1) \tag{72}$$

where $c_1 > 0, m > 0$.

The CAFTSM [13] with NDOB is expressed as

$$i_q^* = -\frac{J}{K_t}\left(u_{eq} + u_b - \hat{D}(t)\right) \tag{73}$$

$$s_3 = \dot{e} + c_2|\dot{e}|^{\alpha_1} sign(\dot{e}) + c_3|\dot{e}|^{\alpha_2} sign(e) \tag{74}$$

$$u_{eq} = \dot{\omega}_m^* + c_2|\dot{e}|^{\alpha_1} sign(\dot{e}) + c_3|\dot{e}|^{\alpha_2} sign(e) \tag{75}$$

$$u_b = \int_0^t \left[g_1 s_3 + g_2 \frac{1 + c_4 - \exp(-c_5|e|)}{c_4} sign(s_3)\right] \tag{76}$$

where $c_2 > 0, c_3 > 0, c_4 > 0, c_5 > 0, 0 < \alpha_1 < \alpha_2 < 2, g_1 > 0, g_2 > 0, \alpha_1 = \frac{p_1}{q_1}, \alpha_1 = \frac{p_2}{q_2}, e = -s_1$, and $\hat{D}_t$ is lumped disturbance observation. p_1, q_1, p_2, and q_2 are odd positive numbers.

TABLE II
PARAMETERS OF CONTROLLER

Symbol	Values
PI controller	$k_p = 12$, $k_i = 0.04$
PI+NDOB	$k_p = 12$, $k_i = 0.04$, $\varepsilon_1 = 800$, $\varepsilon_2 = 1.6\times10^5$, $\phi_1 = 0.78$, $\phi_2 = 0.27$
ISM controller [10]	$c = 10$, $m = 150$
High-gain SOSM [35]	$\hat{\mu}_1 = 2.8$, $\rho_0 = 0.28$
High-gain SOSM+ESO	$\hat{\mu}_2 = 2.8$, $\beta = 6$, $\lambda_5 = 0.45$, $\varepsilon_1 = 800$, $\varepsilon_2 = 1.6\times10^5$
High-gain SOSM+NDOB	$\hat{\mu}_2 = 2.8$, $\beta = 6$, $\lambda_5 = 0.45$, $\varepsilon_1 = 800$, $\varepsilon_2 = 1.6\times10^5$, $\phi_1 = 0.78$, $\phi_2 = 0.27$
CAFTSM+NDOB [13]	$c_2 = 35$, $c_3 = 0.3$, $c_4 = 0.05$, $c_5 = 0.2$, $g_1 = 20$, $g_1 = 60$, $\alpha_1 = 9/7$, $\alpha_2 = 11/7$, $\varepsilon_1 = 800$, $\varepsilon_2 = 1.6\times10^5$, $\phi_1 = 0.78$, $\phi_2 = 0.27$
NASOSM+ESO	$k_1 = 1.8$, $k_2 = 8$, $\alpha = 6$, $\rho_0 = 0.19$, $h = 0.0001$, $L_1 = 2$, $L_2 = 20$, $\varepsilon_1 = 800$, $\varepsilon_2 = 1.6\times10^5$
NASOSM+NDOB	$k_1 = 1.8$, $k_2 = 8$, $\alpha = 6$, $\rho_0 = 0.19$, $h = 0.0001$, $L_1 = 2$, $L_1 = 20$, $\varepsilon_1 = 800$, $\varepsilon_2 = 1.6\times10^5$, $\phi_1 = 0.78$, $\phi_2 = 0.27$

The SOSM controller with high-gain is selected as [35]

$$u_1 = -\mu_1 \cdot sign\left(\lfloor \dot{s}_1 \rfloor^2 + \rho_0^2 \cdot s_1\right). \tag{77}$$

According to (38), the SOSM + ESO/NDOB with high gain is constructed as

$$u_2 = -\lambda_3\left(\left\lfloor s_2 + \hat{d}_1 \right\rfloor^2 + \lambda_5^2 \cdot s_1\right) - \mu_2 \cdot sign\left(\left\lfloor s_2 + \hat{d}_1 \right\rfloor^2 + \lambda_5^2 \cdot s_1\right) \tag{78}$$

where μ_1 μ_2 and λ_5 are positive constant, $\lambda_3 = \beta J/K_t$.

To ensure fairness in comparison, the parameters of inter loops were set identically, the gains of various algorithms can be obtained arbitrarily to get the best performance. The parameters of various controllers were tuned to optimize the performance in terms of comprehensive overshoot, chattering, convergence time, and disturbance rejection. The chosen parameter values for each controller are summarized in Table II. Furthermore, to evaluate chattering, the standard deviation (STD) of the q-axis current ($i_{q\mathrm{STD}}$) was introduced to quantify the steady-state current ripples under each scenario [61]

$$\mathrm{STD} = \sqrt{\frac{1}{N}\sum_{z=1}^{N}\left(i_q(z) - i_{qavg}\right)^2} \tag{79}$$

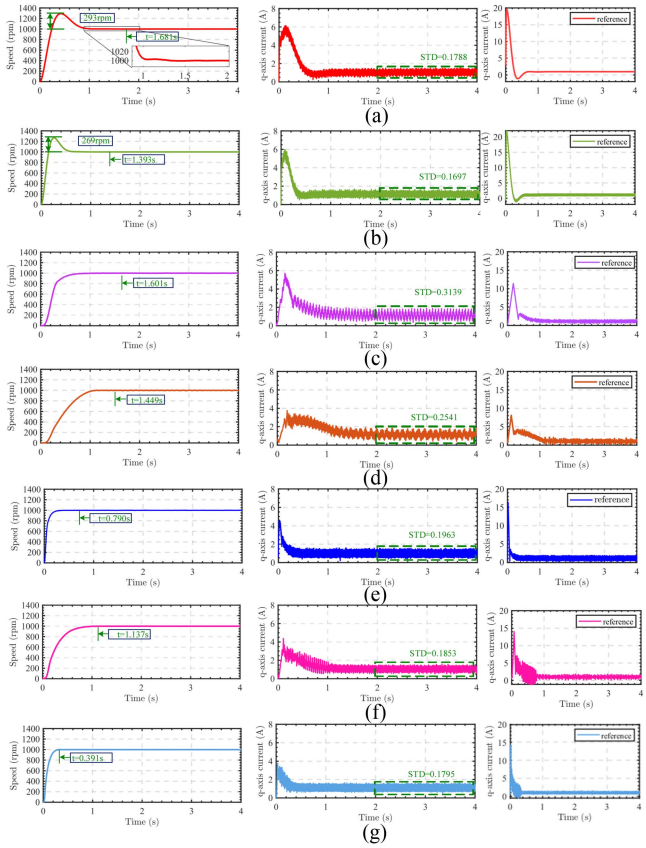

Fig. 5. Experimental results under start-up. (a) PI controller. (b) PI + NDOB. (c) ISM controller. (d) Hign-gain SOSM controller. (e) CAFTSM + NDOB. (f) NASOSM + ESO. (g) NASOSM + NDOB.

where $i_q(z)$ is the instantaneous current value, i_{qavg} is its average, and N is number of sampling points.

The integral of the squared input (ISI) was calculated as an indicator of the control energy [62]

$$\text{ISI} = \sum_{z=1}^{N} i_q^{*\,2}(z) \tag{80}$$

where $i_q^*(z)$ is control input.

The integral of time absolute error (ITAE) [63] was used to evaluate the comprehensive performance of speed response. It is represented as

$$\text{ITAE} = T_s \sum_{z=1}^{N} z\,|\varpi_e|. \tag{81}$$

Remark 15: For the selection of adaptive terms, the appropriate increase of α, ρ_0, and k_1 can effectively reduce the convergence time and enhance the robustness of the system. Excessive increase will cause chattering in the system. The adjustment of k_1 needs to be adjusted to ensure that the system can operate while achieving the steady state with small chattering. The k_2 needs to be debugged to strictly meet the stability conditions, too large k_2 may cause overshooting. The reasonable selection of L_1 and h can ensure the speed and accuracy of the system when it approaches the steady state. The selection of L_2 ensures the rapid increase of $\hat{\mu}$ and prompts the system to achieve finite-time stability.

1) *Start-up Speed Performance Under No-Load:* The reference speed was set at 1000 r/min. As shown in Fig. 5, the PI controller exhibits the largest overshoot and the longest settling time. By adding NDOB, the overshoot caused by the PI controller was reduced, the speed response process was accelerated, and the current ripple was further decreased. SOSM with high-gain, NASOSM + ESO and NASOSM + NDOB demonstrate faster speed response than ISM. Compared with the traditional ISMC, the convergence speed and current indicator of CAFTSM + NDOB has been enhanced. Due to the introduction of adaptive terms and observers, the NASOSM + NDOB achieves the smaller STD value. The introduction of NDOB increases energy consumption to a certain extent. However, since the control gain was not overestimated at steady state, the controller still achieved relatively low energy consumption. By calculating ITAE, the speed from startup to stability was comprehensively evaluated, and the proposed method achieved excellent speed response. The specific performance comparison is presented in Tables III and IV.
2) *Acceleration and Deceleration Under No-Load:* The speed was increased from 800 r/min to 1200 r/min, and then decreased to 1000 r/min. The speed and current responses are illustrated in Fig. 6. The NASOSM + NDOB outperforms other methods in terms of response time, and it achieves excellent current ripple. It can be seen from the control input that even after acceleration and deceleration, the energy consumption of the proposed method still presents an excellent state. Table V summarizes these performance indices.
3) *Speed Response Under Sudden Load Distrubance:* A 0.36 Nm torque distrubance was applied during steady

TABLE III
PERFORMANCE INDEXES OF SEVEN METHODS

Symbol	Setting time (s)	Overshoot (rpm)	Current STD
PI	1.681	293	0.1788
PI+NDOB	1.393	269	0.1697
ISMC [10]	1.601	0	0.3139
High-gain SOSM [35]	1.449	0	0.2541
CAFTSM+NDOB [13]	0.790	0	0.1963
NASOSM+ESO	1.137	0	0.1853
NASOSM+NDOB	**0.391**	**0**	**0.1795**

TABLE IV
PERFORMANCE INDEXES OF SEVEN METHODS

Symbol	ISI	Speed ITAE
PI	589 641	679 009
PI+NDOB	459 744	235 640
ISMC [10]	323 116	503 401
High-gain SOSM [35]	286 356	456 625
CAFTSM+NDOB [13]	121 447	156 836
NASOSM+ESO	167 925	179 689
NASOSM+NDOB	**72 068**	**80 179**

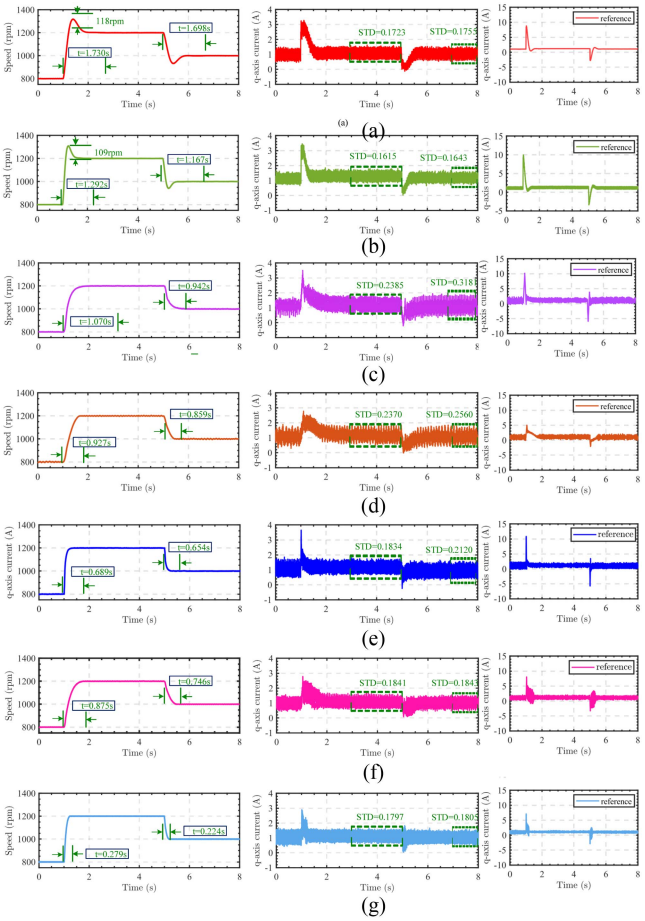

Fig. 6. Speed and q-axis current responses at acceleration and deceleration. (a) PI controller. (b) PI + NDOB. (c) ISM controller. (d) Hign-gain SOSM controller. (e) CAFTSM + NDOB. (f) NASOSM + ESO. (g) NASOSM + NDOB.

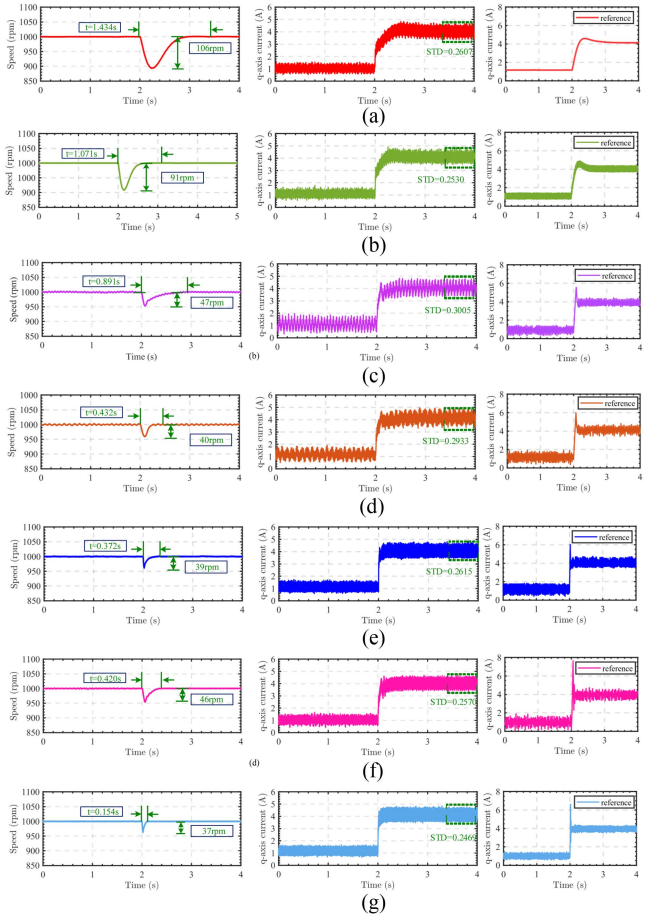

Fig. 7. Experimental results with the load of 0.36 Nm. (a) PI controller. (b) PI + NDOB. (c) ISM controller. (d) Hign-gain SOSM controller. (e) CAFTSM + NDOB. (f) NASOSM + ESO. (g) NASOSM + NDOB.

TABLE V
PERFORMANCE INDEXES OF SEVEN METHODS

Symbol	Acceleration, deceleration time (s)	Overshoot (rpm)	Acceleration, deceleration Current STD
PI	1.730, 1.698	118	0.1723, 0.1755
PI+NDOB	1.292, 1.167	109	0.1615, 0.1643
ISMC [10]	1.070, 0.942	0	0.2385, 0.3181
High-gain SOSM [35]	0.927, 0.859	0	0.2370, 0.2560
CAFTSM+NDOB [13]	0.689, 0.654	0	0.1834, 0.2120
NASOSM+ESO	0.875, 0.746	0	0.1841, 0.1843
NASOSM+NDOB	**0.279, 0.224**	**0**	**0.1797, 0.1805**

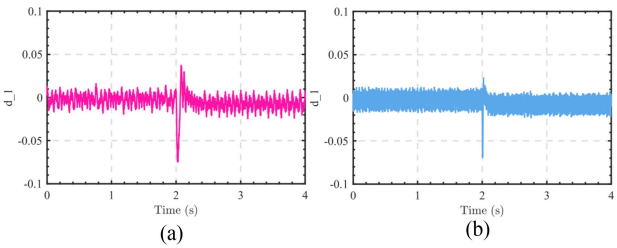

Fig. 8. Uncertainty observation with the load of 0.36 Nm. (a) NASOSM + ESO. (b) NASOSM + NDOB.

operation. It can be seen from Fig. 7 that NASOSM + ESO exhibits the shortest settling time and the smallest drop (37 r/min), indicating strong disturbance rejection. The NASOSM + NDOB outperforms other methods in terms of response time and current ripples when encountering disturbances. In this process, the disturbance observed value have been drawn in Fig. 8. When encountering external disturbances, the combined action of the observer and adaptive terms enhance the robustness of the system. In Fig. 8, the NDOB accelerates the estimation speed and reduces unnecessary fluctuations, further demonstrating the superiority of the proposed observer. The speed ITAE and ISI was calculated, indicating that the proposed method has strong robustness when encountering external disturbances. Tables VI and VII present the quantiatitve results.

4) *Speed Performance Under Rated Speed and Noise:* The reference speed was set at 3000 r/min, and a random noise was applied after 4 s. As shown in Fig. 9, the PI controller is

TABLE VI
PERFORMANCE INDEXES OF SEVEN METHODS

Symbol	Setting time (s)	Speed drop (rpm)	Current STD
PI	1.434	106	0.2607
PI+NDOB	1.071	91	0.2530
ISMC [10]	0.891	47	0.3005
High-gain SOSM [35]	0.432	40	0.2933
CAFTSM+NDOB [13]	0.372	39	0.2615
NASOSM+ESO	0.420	46	0.2570
NASOSM+NDOB	**0.154**	**37**	**0.2469**

TABLE VII
PERFORMANCE INDEXES OF SEVEN METHODS

Symbol	ISI	Speed ITAE
PI	344 860	733 202
PI+NDOB	353 136	563 889
ISMC [10]	382 109	299 895
High-gain SOSM [35]	345 823	189 158
CAFTSM+NDOB [13]	338 812	121 746
NASOSM+ESO	335 352	180 754
NASOSM+NDOB	**331 374**	**118 159**

TABLE VIII
PERFORMANCE INDEXES OF SEVEN METHODS

Symbol	STD	ISI	Speed ITAE
PI	0.2341, 0.2445	220 609	273 374
PI+NDOB	0.2311, 0.2419	244 513	270 121
ISMC [10]	0.2750, 0.3074	215 851	246 453
High-gain SOSM [35]	0.2622, 0.2715	212 508	299 630
CAFTSM+NDOB [13]	0.2572, 0.2705	222 385	188 359
NASOSM+ESO	0.2411, 0.2519	222 212	238 028
NASOSM+NDOB	**0.2398, 0.2451**	**200 048**	**151 619**

relatively sensitive to noise, the steady-state performance of speed is reduced. The control performance of several other methods is affected to some extent by the noise. The NASOSM + ESO still maintains a relatively small speed fluctuation and energy consumption. The specific performance comparison before and after applying noise are calculated respectively and are presented in Table VIII, the proposed method has excellent comprehensive performance

5) *Speed Response Under the Rated Load:* A rated load experiment was carried out to verify the performance of the adaptive term and the NDOB under large disturbances. As shown in Fig. 10, compared with PI, PI + NDOB enhances the anti-interference ability and improves the steady-state accuracy appropriately. Compared with Fig. 10(a), the speed drop in (b) is reduced by 29 r/min, and it has a smaller current ripple. In Fig. 10(c), (d), (f), and (g), it also

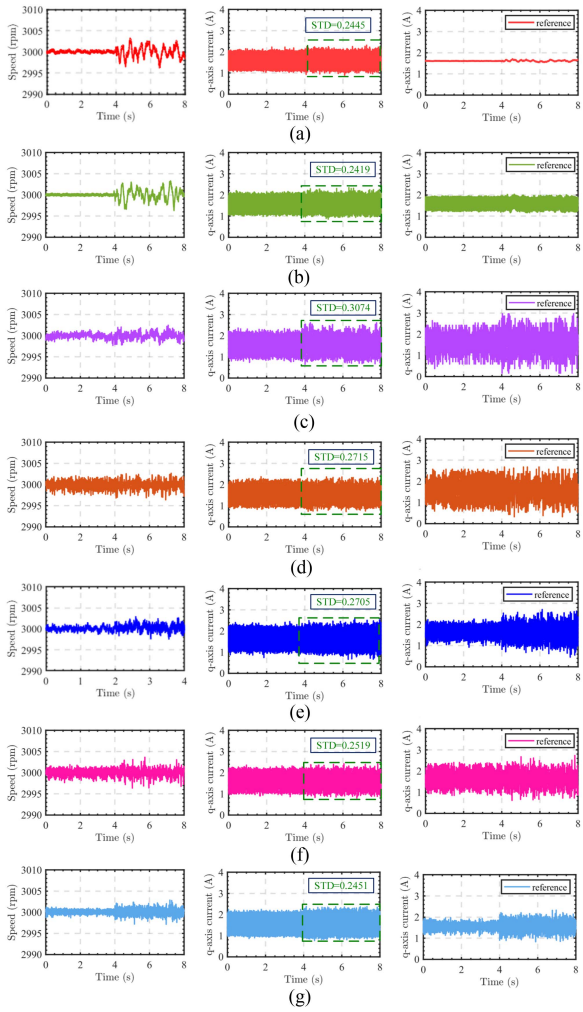

Fig. 9. Experimental results under rated Speed. (a) PI controller. (b) PI + NDOB. (c) ISM controller. (d) Hign-gain SOSM controller. (e) CAFTSM + NDOB. (f) NASOSM + ESO. (g) NASOSM + NDOB.

TABLE IX
PERFORMANCE INDEXES OF SEVEN METHODS

Symbol	Setting time (s)	Speed drop (rpm)	Current STD
PI	0.942	295	/
PI+NDOB	1.931	256	/
High-gain SOSM+ESO	0.940	281	0.3723
High-gain SOSM+NDOB	0.302	239	0.3680
CAFTSM+NDOB [13]	0.693	177	0.3554
NASOSM+ESO	0.834	227	0.3491
NASOSM+NDOB	**0.251**	**173**	**0.3485**

verifies that the adaptive terms further enhance both dynamic and steady-state performance. By integrating the six schemes, the proposed NASOSM + NDOB has the fastest response of 0.251 s, the least speed drop of 173 r/min and the smallest current ripple, which achieves fast and stable operation under large disturbances. To further analyze the superiority of the adaptive terms and the observer, performance metrics are presented in Table IX.

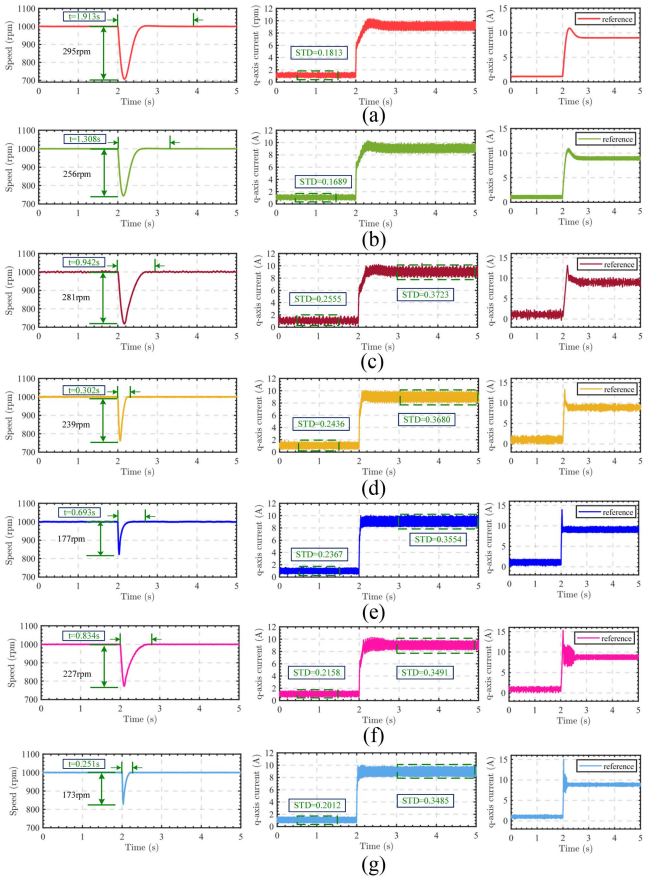

Fig. 10. Experimental results with the rated load. (a) PI controller. (b) PI + NDOB. (c) SOSM + ESO. (d) SOSM + NDOB. (e) CAFTSM + NDOB. (f). NASOSM + ESO. (g) NASOSM + NDOB.

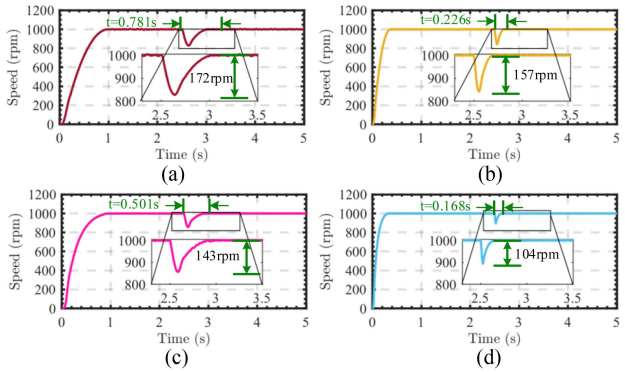

Fig. 11. Speed responses under 0.5J parameter mismatch. (a) SOSM + ESO. (b) SOSM + NDOB. (c) NASOSM + ESO. (d) NASOSM + NDOB.

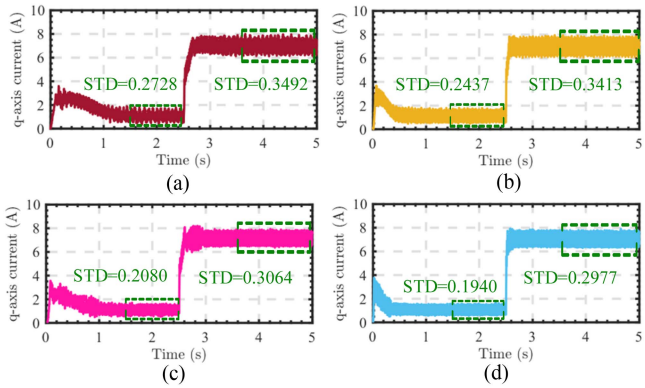

Fig. 12. q-axis current responses under 0.5 J parameter mismatch. (a) SOSM + ESO. (b) SOSM + NDOB. (c) NASOSM + ESO. (d) NASOSM + NDOB.

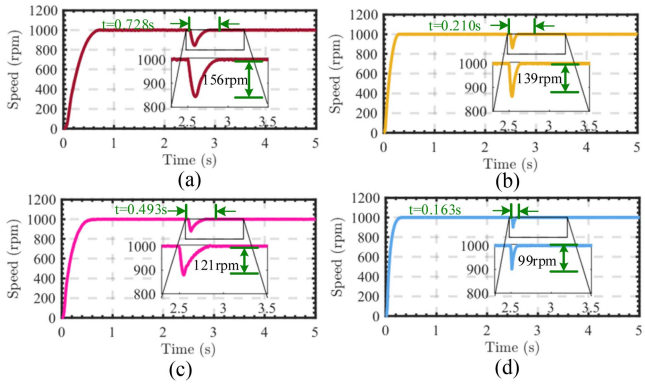

Fig. 13. Speed responses under 1.5J parameter mismatch. (a) SOSM + ESO. (b) SOSM + NDOB. (c) NASOSM + ESO. (d) NASOSM + NDOB.

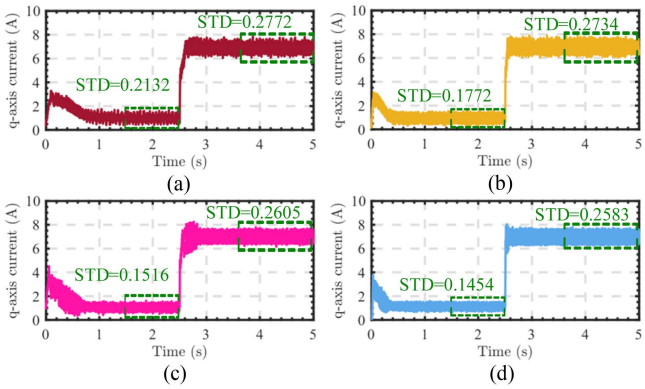

Fig. 14. q-axis current responses under 1.5J parameter mismatch. (a) SOSM + ESO. (b) SOSM + NDOB. (c) NASOSM + ESO. (d) NASOSM + NDOB.

6) *Uncertainty Under Parameter Mismatch:* The inertia mismatch affects the robustness of SPMSM. Set the inertia to 0.5 J and 1.5 J, and observe the performance of four methods. The reference speed was set to 1000 r/min, and a load disturbance of 0.7 Nm was given in the 2.5 s. Shown in Figs. 11 –14, it can be seen that the proposed method has excellent control performance under parameter uncertainty, and the adaptive terms and observer under the proposed framework provide a guarantee for the overall performance of the system. The control effect of the NASOSM + NDOB is better than that of other methods. In Fig. 15, the perturbation observations were recorded. The NDOB can observe the uncertainty quickly and smoothly. The performance of four methods is summarized in Tables X and XI.

7) *Adaptive Terms Analysis:* For the NASOSM + NDOB, the dynamic adjustment of the adaptive terms was plotted under various operating conditions. As can be seen

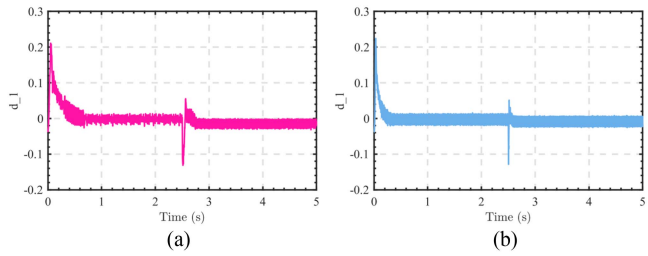

Fig. 15. Uncertainty observation under $1.5J$ parameter mismatch. (a) NASOSM + ESO. (b) NASOSM + NDOB.

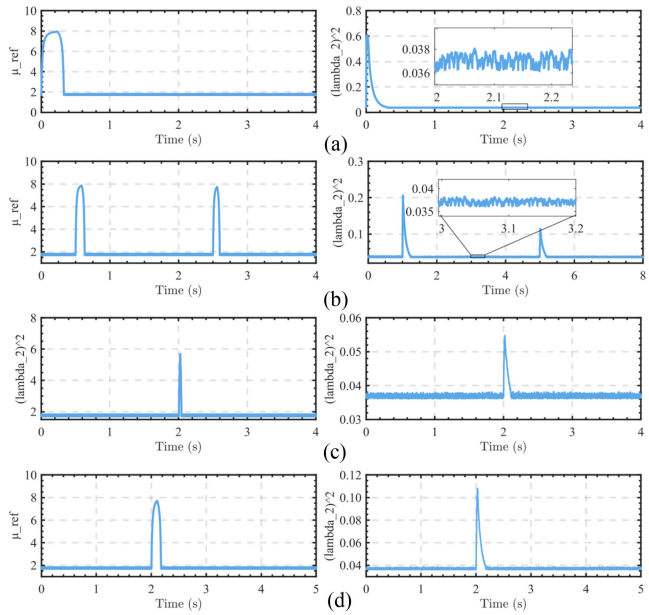

Fig. 16. Adaptive term variation under multiple operating conditions. (a) Start-up. (b) Acceleration and deceleration. (c) Sudden 0.36 Nm load disturbance. (d) Rated load.

TABLE X
PERFORMANCE INDEXES OF FOUR METHODS AT 0.5 J

Symbol	Setting time (s)	Speed drop (rpm)	Current STD
SOSM+ESO	0.781	172	0.2728, 0.3492
SOSM+NDOB	0.226	157	0.2437, 0.3413
NASOSM+ESO	0.501	143	0.2080, 0.3064
NASOSM+NDOB	**0.168**	**104**	**0.1940, 0.2977**

in Fig. 16, when the motor start-up, the adaptive term gradually increases, and after reaching the predetermined area, it gradually decreases and remains at a small gain. Acceleration and deceleration also dynamically adjust the gain according to the set rules. In Fig. 16(c) and (d), when encountering external disturbances, a transient large gain can quickly drive the motor speed to the reference value, greatly enhancing the robustness of the motor system. The adaptive term enables the motor to achieve rapid response while ensuring high-precision operation.

1) *Computational Burden Analysis:* The computational burden of the SMC methods involved is compared and analyzed. Breakpoints are inserted at the beginning and end of each interrupt triggered in each control cycle in order to measure the number of clock cycles consumed. The results are summarized in Table XII. Although the proposed control method imposes a relatively heavy computational burden, its execution time remains significantly shorter than the 1 ms sampling period, enabling it to accomplish the control task of speed loop.

TABLE XI
PERFORMANCE INDEXES OF FOUR METHODS AT 1.5 J

Symbol	Setting time (s)	Speed drop (rpm)	Current STD
SOSM+ESO	0.728	156	0.2123, 0.2772
SOSM+NDOB	0.210	139	0.1772, 0.2734
NASOSM+ESO	0.493	121	0.1516, 0.2605
NASOSM+NDOB	**0.163**	**99**	**0.1454, 0.2583**

TABLE XII
COMPUTATIONAL BURDEN OF SEVEN METHODS

Symbol	Execution time (μs)
ISMC [10]	5.77
High-gain SOSM [35]	5.33
High-gain SOSM+ESO	5.92
High-gain SOSM+NDOB	6.68
CAFTSM+NDOB [13]	8.36
NASOSM+ESO	12.48
NASOSM+NDOB	**13.82**

V. CONCLUSION

In this work, a new NASOSM controller combined with NDOB was proposed for SPMSM systems to enhance speed tracking performance under uncertainties. The presented NASOSM controller address the gain overestimation, and enhances robustness while reducing chattering. The NDOB further improves the system's adaptability to disturbances, enabling accurate and fast tracking. The proposed composite control method enhances the system's speed response, minimizes current fluctuations during steady-state operation, and ensures excellent robustness under uncertain conditions. Even when the system encounters large disturbances, the proposed method can ensure the rapid response of the system and meet the balance between robustness and control accuracy. Experimental results confirm the effectiveness of the proposed method across various operating conditions of SPMSM. In future work, the current loop should be considered to reduce the current harmonic component. Weakening system noise and reducing the computational burden will also be further concentrated.

REFERENCES

[1] G. Wang, M. Valla, and J. Solsona, "Position sensorless permanent magnet synchronous machine drives - A review," *IEEE Trans. Ind. Electron.*, vol. 67, no. 7, pp. 5830–5842, Jul. 2020.

[2] T. H. Nguyen, T. T. Nguyen, V. Q. Nguyen, K. M. Le, H. N. Tran, and J. W. Jeon, "An adaptive sliding-mode controller with a modified reduced-order proportional integral observer for speed regulation of a permanent magnet synchronous motor," *IEEE Trans. Ind. Electron.*, vol. 69, no. 7, pp. 7181–7191, Jul. 2022.

[3] Z. Yin, L. Gong, C. Du, J. Liu, and Y. Zhong, "Integrated position and speed loops under sliding-mode control optimized by differential evolution algorithm for PMSM drives," *IEEE Trans. Power Electron.*, vol. 34, no. 9, pp. 8994–9005, Sep. 2019.

[4] Y. Ma, D. Li, Y. Li, and L. Yang, "A novel discrete compound integral terminal sliding mode control with disturbance compensation for PMSM speed system," *IEEE/ASME Trans. Mechatron.*, vol. 27, no. 1, pp. 549–560, Feb. 2022.

[5] W. Xu, A. K. Junejo, Y. Liu, M. G. Hussien, and J. Zhu, "An efficient antidisturbance sliding-mode speed control method for PMSM drive systems," *IEEE Trans. Power Electron.*, vol. 36, no. 6, pp. 6879–6891, Jun. 2021.

[6] S. Li and H. Gu, "Fuzzy adaptive internal model control schemes for PMSM speed-regulation system," *IEEE Trans. Ind. Inform.*, vol. 8, no. 4, pp. 767–779, Nov. 2012.

[7] L. He, F. Wang, and D. Ke, "FPGA-based sliding-mode predictive control for PMSM speed regulation system using an adaptive ultralocal model," *IEEE Trans. Power Electron.*, vol. 36, no. 5, pp. 5784–5793, May 2021.

[8] H. Du, G. Wen, Y. Cheng, and J. Lv, "Design and implementation of bounded finite-time control algorithm for speed regulation of permanent magnet synchronous motor," *IEEE Trans. Ind. Electron.*, vol. 68, no. 3, pp. 2417–2426, Mar. 2021.

[9] S. Li, H. Won, X. Fu, M. Fairbank, D. C. Wunsch, and E. Alonso, "Neural-network vector controller for permanent-magnet synchronous motor drives: Simulated and hardware-validated results," *IEEE Trans. Cybern.*, vol. 50, no. 7, pp. 3218–3230, Jul. 2020.

[10] Q. Hou, S. Ding, and X. Yu, "Composite super-twisting sliding mode control design for PMSM speed regulation problem based on a novel disturbance observer," *IEEE Trans Energy Convers*, vol. 36, no. 4, pp. 2591–2599, Dec. 2021.

[11] Z. Zhang and X. Liu, "An improved super-twisting sliding mode single-loop control with current-constraint for PMSM based on two-time scale disturbance observer," *IEEE Trans. Transport. Electrific.*, vol. 10, no. 3, pp. 5389–5399, Sep. 2024.

[12] S. Shi, L. Dai, H. Min, J. Yang, and S. Li, "Prescribed-time nonsingular terminal sliding mode control and its application in PMSM servo systems," *IEEE Trans. Ind. Electron.*, vol. 72, no. 3, pp. 3072–3081, Mar. 2025.

[13] L. Chen, H. Zhang, H. Wang, K. Shao, G. Wang, and A. Yazdani, "Continuous adaptive fast terminal sliding mode-based speed regulation control of PMSM drive via improved super-twisting observer," *IEEE Trans. Ind. Electron.*, vol. 71, no. 5, pp. 5105–5115, May 2024.

[14] M. Tian, T. Wang, Y. Yu, Q. Dong, B. Wang, and D. Xu, "Integrated observer-based terminal sliding-mode speed controller for PMSM drives considering multisource disturbances," *IEEE Trans Power Electron*, vol. 39, no. 7, pp. 7968–7979, Jul. 2024.

[15] Q. Xu, "Precision motion control of piezoelectric nanopositioning stage with chattering-free adaptive sliding mode control," *IEEE Trans. Autom. Sci. Eng.*, vol. 14, no. 1, pp. 238–248, Jan. 2017.

[16] J. Liu et al., "Sliding mode control of grid-connected neutral-point-clamped converters via high-gain observer," *IEEE Trans. Ind. Electron.*, vol. 69, no. 4, pp. 4010–4021, Apr. 2022.

[17] C. Baik, K. H. Kim, and M. J. Youn, "Robust nonlinear speed control of PM synchronous motor using boundary layer integral sliding modecontrol technique," *IEEE Trans. Control Syst. Technol.*, vol. 8, no. 1, pp. 47–54, Jan. 2000.

[18] H. Wang et al., "Continuous fast nonsingular terminal sliding mode control of automotive electronic throttle systems using finite-time exact observer," *IEEE Trans. Ind. Electron.*, vol. 65, no. 9, pp. 7160–7172, Sep. 2018.

[19] S. Li, M. Zhou, and X. Yu, "Design and implementation of terminal sliding mode control method for PMSM speed regulation system," *IEEE Trans. Ind. Inform.*, vol. 9, no. 4, pp. 1879–1891, Nov. 2013.

[20] D. Kong, H. Cai, and H. Zhai, "Double-layer fast terminal sliding mode predictive control for PMSM speed regulation," *IEEE J. Emerg. Sel. Topics Power Electron.*, vol. 12, no. 5, pp. 4876–4887, Oct. 2024.

[21] K. Zhao et al., "Model-free fast integral terminal sliding-mode control method based on improved fast terminal sliding-mode observer for PMSM with unknown disturbances," *ISA Trans*, vol. 143, pp. 572–581, Dec. 2023.

[22] B. Xu, L. Zhang, and W. Ji, "Improved non-singular fast terminal sliding mode control with disturbance observer for PMSM drives," *IEEE Trans. Transport. Electrific.*, vol. 7, no. 4, pp. 2753–2762, Dec. 2021.

[23] Z. Yang, J. Sun, X. Sun, B. Wang, and L. Feng, "Direct instantaneous torque control for six-phase SRM with nonsingular fast terminal sliding mode controller," *IEEE J. Emerg. Sel. Topics Power Electron.*, vol. 12, no. 1, pp. 505–515, Feb. 2024.

[24] J. Wang, J. Rong, and J. Yang, "Adaptive fixed-time position precision control for magnetic levitation systems," *IEEE Trans. Autom. Sci. Eng.*, vol. 20, no. 1, pp. 458–469, Jan. 2023.

[25] L. Chen et al., "Sensorless fixed-time sliding mode control of PMSM based on barrier function adaptive super-twisting observer," *IEEE Trans. Power Electron.*, vol. 39, no. 3, pp. 3037–3051, Mar. 2024.

[26] C. Jia, X. Liu, X. Li, and J. Xu, "A new adaptive predefined time sliding mode control for nonlinear systems," *IEEE Trans. Circuits Syst. II, Exp. Briefs*, vol. 71, no. 4, pp. 2094–2098, Apr. 2024.

[27] S. Ding, A. Levant, and S. Li, "Simple homogeneous sliding-mode controller," *Automatica*, vol. 67, no. 5, pp. 22–32, May 2016.

[28] Z. Lv, Y. Wu, X. M. Sun, and Q. G. Wang, "Fixed-time control for a quadrotor with a cable-suspended load," *IEEE Trans. Intell. Transp. Syst.*, vol. 23, no. 11, pp. 21932–21943, Nov. 2022.

[29] S. Ding, K. Mei, and S. Li, "A new second-order sliding mode andits application to nonlinear constrained systems," *IEEE Trans. Autom. Control*, vol. 64, no. 6, pp. 2545–2552, Jun. 2019.

[30] A. Levant, "Sliding order and sliding accuracy in sliding mode control," *Int. J. Control*, vol. 58, no. 6, pp. 1247–1263, Dec. 1993.

[31] A. Levant, "Principles of 2-sliding mode design," *Automatica*, vol. 43, no. 4, pp. 576–586, Apr. 2007.

[32] V. Utkin, "On convergence time and disturbance rejection of supertwisting control," *IEEE Trans. Autom. Control*, vol. 58, no. 8, pp. 2013–2017, Aug. 2013.

[33] Q. Hou and S. Ding, "GPIO based super-twisting sliding mode control for PMSM," *IEEE Trans. Circuits Syst. II, Exp. Briefs*, vol. 68, no. 2, pp. 747–751, Feb. 2021.

[34] Y. Chen and X. Liu, "A variable rate supertwisting sliding mode speed control with overcurrent protection for PMSM considering aperiodic and periodic disturbances," *IEEE Trans. Power Electron.*, vol. 40, no. 4, pp. 5787–5798, Apr. 2025.

[35] S. Ding, W. X. Zheng, J. Sun, and J. Wang, "Second-order sliding-mode controller design and its implementation for buck converters," *IEEE Trans. Ind. Inform.*, vol. 14, no. 5, pp. 1990–2000, May 2018.

[36] M. Behnamfar, T. O. Olowu, M. Tariq, A. Debnath, and A. Sarwat, "Composite second-order sliding mode and backstepping control for power pulsation suppression in dynamic wireless charging," *IEEE Trans. Ind. Appl.*, vol. 60, no. 4, pp. 5803–5812, Jul./Aug. 2024.

[37] K. Mei, S. Ding, and X. Yu, "A generalized supertwisting algorithm," *IEEE Trans. Cybern.*, vol. 53, no. 6, pp. 3951–3960, Jun. 2023.

[38] L. Zhang et al., "An adaptive backstepping sliding mode controller to improve vehicle maneuverability and stability via torque vectoring control," *IEEE Trans. Veh. Technol.*, vol. 69, no. 3, pp. 2598–2612, Mar. 2020.

[39] G. P. Incremona, M. Cucuzzella, and A. Ferrara, "Adaptive suboptimal second-order sliding mode control for microgrids," *Int. J. Control*, vol. 89, no. 9, pp. 1849–1867, Jan. 2016.

[40] Y. Shtessel, M. Taleb, and F. Plestan, "A novel adaptive-gain supertwisting sliding mode controller: Methodology and application," *Automatica*, vol. 48, no. 5, pp. 759–769, 2012.

[41] X. Shen et al., "Adaptive second-order sliding mode control for grid-connected NPC converters with enhanced disturbance rejection," *IEEE Trans. Power Electron.*, vol. 37, no. 1, pp. 206–220, Jan. 2022.

[42] H. Obeid, S. Laghrouche, L. Fridman, Y. Chitour, and M. Harmouche, "Barrier function-based adaptive super-twisting controller," *IEEE Trans. Autom. Control*, vol. 65, no. 11, pp. 4928–4933, Nov. 2020.

[43] Y. Zheng, J. Zheng, K. Shao, H. Zhao, H. Xie, and H. Wang, "Adaptive trajectory tracking control for nonholonomic wheeled mobile robots: A barrier function sliding mode approach," *IEEE/CAA J. Autom. Sinica*, vol. 11, no. 4, pp. 1007–1021, Apr. 2024.

[44] P. Li, X. Yu, and B. Xiao, "Adaptive quasi-optimal higher order sliding mode control without gain overestimation," *IEEE Trans. Ind. Inform.*, vol. 14, no. 9, pp. 3881–3891, Sep. 2018.

[45] S. Ding, Q. Hou, and H. Wang, "Disturbance-observer-based second-order sliding mode controller for speed control of PMSM drives," *IEEE Trans. Energy Convers.*, vol. 38, no. 1, pp. 100–110, Mar. 2023.

[46] J. Yim, S. You, Y. Lee, and W. Kim, "Chattering attenuation disturbance observer for sliding mode control: Application to permanent magnet synchronous motors," *IEEE Trans. Ind. Electron.*, vol. 70, no. 5, pp. 5161–5170, May 2023.

[47] L. Qu, W. Qiao, and L. Qu, "An extended-state-observer-based sliding-mode speed control for permanent-magnet synchronous motors," *IEEE J. Emerg. Sel. Topics Power Electron.*, vol. 9, no. 2, pp. 1605–1613, Apr. 2021.

[48] W. Xu, A. K. Junejo, Y. Liu, and M. R. Islam, "Improved continuous fast terminal sliding mode control with extended state observer for speed regulation of PMSM drive system," *IEEE Trans. Veh. Technol.*, vol. 68, no. 11, pp. 10465–10476, Nov. 2019.
[49] J. Yang, X. Yu, L. Zhang, and S. Li, "A Lyapunov-based approach for recursive continuous higher order nonsingular terminal sliding-mode control," *IEEE Trans. Autom. Control.*, vol. 66, no. 9, pp. 4424–4431, Sep. 2021.
[50] S. Ding, K. Mei, and X. Yu, "Adaptive second-order sliding mode control: A Lyapunov approach," *IEEE Trans. Autom. Control*, vol. 67, no. 10, pp. 5392–5399, Oct. 2022.
[51] C. Lei, J. Nan, C. Shaoping, Z. Zhiqiang, and Z. Zhengen, "Fixed-time ESO based fixed-time integral terminal sliding mode controller design for a missile," *ISA Trans.*, vol. 125, pp. 237–251, Jun. 2022.
[52] A. Polyakov, "Nonlinear feedback design for fixed-time stabilization of linear control systems," *IEEE Trans. Autom. Control*, vol. 57, no. 8, pp. 2106–2110, Aug. 2012.
[53] W. Yang, S. Ding, and C. Ding, "Fast supertwisting sliding mode control with antipeaking extended state observer for path-tracking of unmanned agricultural vehicles," *IEEE Trans. Ind. Electron.*, vol. 71, no. 10, pp. 12973–12982, Oct. 2024.
[54] Z. Zhang and X. Liu, "An improved super-twisting sliding mode single-loop control with current-constraint for PMSM based on two-time scale disturbance observer," *IEEE Trans. Transport. Electrific.*, vol. 10, no. 3, pp. 5389–5399, Sep. 2024.
[55] B. Jiang, Q. Hu, and M. I. Friswell, "Fixed-time rendezvous control of spacecraft with a tumbling target under loss of actuator effectiveness," *IEEE Trans. Aero. Electron. Sys.*, vol. 52, no. 4, pp. 1576–1586, Aug. 2016.
[56] Q. Hou, S. Ding, X. Yu, and K. Mei, "A super-twisting-like fractional controller for SPMSM drive system," *IEEE Trans. Ind. Electron.*, vol. 69, no. 9, pp. 9376–9384, Sep. 2022.
[57] X. Wang and S. Wang, "Fixed-time integral terminal sliding-mode control with super-twisting nonlinear extended-state observer for servo system with disturbances," *IEEE J. Emerg. Sel. Topics Ind. Electron.*, vol. 6, no. 1, pp. 435–446, Jan. 2025.
[58] Q. Hou, H. Wang, C. H. T. Lee, and S. Ding, "Composite adaptive super-twisting sliding mode control using barrier function for PM motor drives toward electric aircraft applications," *IEEE Trans Power Electron*, vol. 40, no. 11, pp. 16255–16264, Nov. 2025.
[59] L. Zhao, S. Gu, J. Zhang, and S. Li, "Finite-time trajectory tracking control for rodless rneumatic cylinder systems with disturbances," *IEEE Trans. Ind. Electron.*, vol. 69, no. 4, pp. 4137–4147, Apr. 2022.
[60] A. K. Junejo, W. Xu, C. Mu, M. M. Ismail, and Y. Liu, "Adaptive speed control of PMSM drive system based a new sliding-mode reaching law," *IEEE Trans. Power Electron.*, vol. 35, no. 11, pp. 12110–12121, Nov. 2020.
[61] Y. Xu, Z. Yan, Y. Zhang, and R. Song, "Model predictive current control of permanent magnet synchronous motor based on sliding mode observer with enhanced current and speed tracking ability under disturbance," *IEEE Trans. Energy Convers.*, vol. 38, no. 2, pp. 948–958, Jun. 2023.
[62] N. Aguila-Camacho and M. A. Duarte-mermoud, "Improving the control energy in model reference adaptive controllers using fractional adaptive laws," *IEEE/CAA J. Autom. Sinica*, vol. 3, no. 3, pp. 332–337, Jul. 2016.
[63] Y. Wei, Y. Wei, Y. Sun, H. Qi, X. Guo, and M. Li, "A smith structure-based delay compensation method for model predictive current control of PMSM system," *IEEE J. Emerg. Sel. Topics Power Electron.*, vol. 10, no. 4, pp. 4090–4101, Aug. 2022.

Cao Li was born in Anhui, China, in 1997. He is currently working toward the Ph.D. degree in electrical engineering with the School of Electrical Engineering and Automation, Anhui University, Hefei, China.

His research interests include sliding mode control and its application to permanent magnet synchronous motor.

Tianhong Pan (Senior Member, IEEE) received the Ph.D. degree in control theory and control engineering from Shanghai Jiaotong University, Shanghai, China, in 2007.

He is currently working toward the Professor with the School of Electrical Engineering and Automation, Anhui University, Hefei, China. His research interests include multiple model approach and its application, machine learning, virtual metrology, predictive control, and run-to-run control theory.

Shihong Ding (Senior Member, IEEE) was born in Anhui, China, in 1983. He received the B.E. degree in mathematics from Anhui Normal University, Wuhu, China, in 2004, and the M.S. and Ph.D. degrees in automatic control from Southeast University, Nanjing, China, in 2007 and 2010, respectively.

During the graduate studies, he visited The University of Texas at San Antonio, San Antonio, TX, USA, from 2008 to 2009. After graduation, he held a Research Fellowship with the University of Western Sydney, Penrith, Australia, for one year. He also visited Yeungnam University, Gyeongsan, South Korea, from July to August 2018, and RMIT University, Melbourne, VIC, Australia, from 2019 to 2020, respectively. Since 2010, he has been with the School of Electrical and Information Engineering, Jiangsu University, Zhenjiang, China, where he is currently a Full Professor. His research interests include sliding mode control and finite-time stability.

Liming Qian received the Ph.D. degree in mechanical and electrical engineering from the University of Science and Technology of China, Hefei, China, in 2004.

He is a Senior Engineer. He has engaged in the operation, maintenance, and management of electromechanical equipment for a long time.